This article has been accepted for publication in IEEE Sensors Journal. This is the author's version which has not been fully edited and content may change prior to final publication. Citation information: DOI 10.1109/JSEN.2025.3545789

Precision Multi-Band Terahertz Metamaterial Biosensor with Targeted Spectral Selectivity for Early Detection of MCF-7 Breast Cancer Cells

Musa N. Hamza, Mohammad Alibakhshikenari, Bal Virdee, Sunil Lavadiya, Iftikhar ud Din, Bruno Sanches, Slawomir Koziel, Syeda Iffat Naqvi, Abinash Panda, Ali Farmani, Nasr Rashid, Lida Kouhalvandi and Milad Shariatifar

***Abstract*— Cancer remains one of the leading causes of mortality worldwide, with breast cancer being a particularly prevalent form. Projections estimate nearly 20 million new cases globally over the next two decades. Early detection is critical for effective treatment; however, conventional diagnostic techniques often lack the necessary sensitivity and specificity, with some methods being invasive and labor-intensive. Recent advancements in microwave imaging (MWI) have shown significant potential as efficient, non-invasive tools for monitoring various cancer types. MWI operating in the terahertz (THz) range has emerged as a promising approach for bio-sensing, offering the precision needed to differentiate between healthy and cancerous tissues by analyzing small-scale biological features. Among the methods for breast cancer detection, the identification and analysis of MCF-7 breast cancer cells are particularly significant. THz waves interact uniquely with the intrinsic properties of MCF-7 cells, making THz-based biosensors ideal candidates for diagnostic tools. However, many existing sensors are limited in key performance areas, including operating bandwidth and absorption efficiency. This study introduces a novel multi-band metamaterial (MTM)-based biosensor specifically designed for the detection of MCF-7 breast cancer cells. The sensor features a compact geometry composed of multiple resonators made from 200-nm-thick aluminum (Al) layers on a 50-µm-thick polyethylene terephthalate (PET) substrate. With dimensions of only 198 × 198 µm², the proposed device is exceptionally compact. It operates in the 0.5 THz to 1.6 THz frequency range and achieves near-perfect absorption rates (>99%) across multiple bandwidths. These results are achieved through precise tuning of the sensor's geometry and architectural optimization, significantly enhancing its sensitivity for cancer detection. Comprehensive validation of the sensor is performed using full-wave electromagnetic analysis, which includes evaluating electric and magnetic field distributions, surface currents, and scattering parameters. Extensive benchmarking demonstrates the device's superior performance compared to state-of-the-art biosensors, excelling in metrics such as quality-factor, figure of merit (FOM), and absorption efficiency. Additionally, the proposed sensor has been integrated into an MWI system to evaluate its practical application. The device successfully discriminated against subtle changes in the refractive index of biological tissues, confirming its ability to detect MCF-7 cells effectively. These findings highlight the sensor's suitability as a non-invasive, early-stage diagnostic tool for breast cancer.**

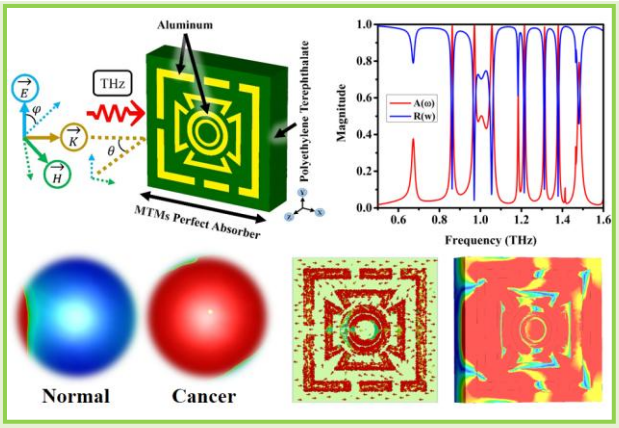

***Index Terms*— Terahertz Biosensor; Multi-Band Metamaterial; MCF-7 Breast Cancer Detection; Microwave Imaging (MWI); Non-Invasive Cancer Diagnosis**

I. Introduction

Cancer remains one of the most prevalent and fatal diseases worldwide, impacting millions of lives each year [1, 2]. According to the World Health Organization (WHO), global cancer data from 2020 indicated approximately 19.29 million new cases and 9.96 million deaths due to cancer [1, 3, 4]. This prevalence highlights the disease's substantial role as a barrier to increasing life expectancy globally. By 2040, the number of new cancer cases is expected to escalate to 28.4 million,

This work is partially supported by the Icelandic Research Fund Grant 2410297 and by National Science Centre of Poland Grant 2022/47/B/ST7/00072. (Corresponding authors: Musa N. Hamza and Mohammad Alibakhshikenari)

Musa N. Hamza is with the Department of Physics, College of Science, University of Raparin, Sulaymaniyah 46012, Iraq; (e-mail: musa.nuraden@uor.edu.krd)

Mohammad Alibakhshikenari and Milad Shariatifar are with the Department of Electronics Engineering, University of Rome "Tor Vergata", 00133 Rome, Italy; (e-mail: alibakhshikenari@ing.uniroma2.it and milad.shariatifar@uniroma2.it)

Bal Virdee is with the Department of Center for Communications Technology, London Metropolitan University, London N7 8DB, United Kingdom; (e-mail: b.virdee@londonmet.ac.uk)

Sunil Lavadiya is with the Department of Information and Communication Technology, Marwadi University, Rajkot-360003, Gujarat, India; (e-mail: sunil.lavadiya@marwadieducation.edu.in)

Iftikhar ud Din is with the Department of Telecommunication Engineering, University of Engineering and Technology, Mardan 23200, Pakistan; (e-mail: iftikharuddin114@gmail.com)

Bruno Sanches is with Department of Electronic Systems Engineering, Escola Politécnica da Universidade de São Paulo São Paulo, Brazil; (e-mail: bruno.csanches@usp.br)

Slawomir Koziel is with Engineering Optimization & Modeling Center, Reykjavik University, 102 Reykjavik, Iceland, he is also with Faculty of Electronics, Telecommunications and Informatics, Gdansk University of Technology, 80-233 Gdansk, Poland; (e-mail: Koziel@ru.is)

Syeda Iffat Naqvi is with the Department of Telecommunication Engineering University of Engineering & Technology Taxila, Pakistan; (e-mail: iffat.naqvi@uettaxila.edu.pk)

Abinash Panda is with the Department of Electronics and Communication Engineering, CMR Institute of Technology, Bengaluru 560037, India; (e-mail: abinashpanda087@gmail.com)

Ali Farmani is with the Department of Electronics engineering, Lorestan University, Iran; (e-mail: farmani.a@lu.ac.ir)

Nasr Rashid is with the Department of Electrical Engineering, College of Engineering, Jouf University, Sakaka, Aljouf 72388, Saudi Arabia, also he is with the Department of Electrical Engineering, Faculty of Engineering, Al-Azhar University, Nasr City, Cairo 11884, Egypt; (e-mail: nasrrashid34.el@azhar.edu.eg)

Lida Kouhalvandi is with Department of Electrical and Electronics Engineering, Dogus University, Istanbul 34775, Turkiye; (e-mail: lida.kouhalvandi@ieee.org)

XXXX-XXXX © XXXX IEEE. Personal use is permitted, but republication/redistribution requires IEEE permission.
See http://www.ieee.org/publications_standards/publications/rights/index.html for more information.
Authorized licensed use limited to: London Metropolitan University. Downloaded on March 14,2025 at 11:16:28 UTC from IEEE Xplore. Restrictions apply.
© 2025 IEEE. All rights reserved, including rights for text and data mining and training of artificial intelligence and similar technologies. Personal use is permitted,
but republication/redistribution requires IEEE permission. See https://www.ieee.org/publications/rights/index.html for more information.

This article has been accepted for publication in IEEE Sensors Journal. This is the author's version which has not been fully edited and
content may change prior to final publication. Citation information: DOI 10.1109/JSEN.2025.3545789

reflecting a growing health challenge. The five deadliest types of cancer, i.e. lung, colorectal, liver, stomach, and breast cancer are accounted for significant mortality rates in 2020. In particular, Breast cancer (BC) remains a leading cause of cancer-related deaths [5, 6]. Breast cancer remains a significant global health challenge, accounting for 626,679 deaths among the 2.1 million newly reported cases in 2018 alone [7]. As the incidence of breast cancer continues to rise, projections suggest an increase in the number of cases worldwide, from 14 million to 22 million over the next 20 years [8, 9]. This rise in cases is influenced by factors such as limited access to healthcare, late-stage diagnoses, and inadequate cancer awareness programs. Early detection of breast cancer significantly improves survival rates by enabling timely and less invasive treatments [10]. Recognizing cancer cells at their earliest stages is vital for diagnosing and addressing the disease before it progresses or metastasizes [11].

The high mortality rate of cancer can be reduced by early and accurate diagnosis; hence, rapid and sensitive detection of tumor markers in complex biological samples is of great demand for the early diagnosis of malignancy in clinical laboratories. While tissue biopsy remains the gold standard for cancer diagnosis, its accuracy is limited by sampling error, as only small portions of the lesion tissue are analyzed. Guiding techniques for tissue biopsy, such as Magnetic Resonance Imaging (MRI) [12] and White Light Reflectance (WLR) [13], offer valuable diagnostic insights and help minimize biopsy-related trauma. However, these methods have low specificity, often requiring contrast agents to enhance detection. Moreover, they provide limited or no information about the cellular and molecular characteristics of tumors. Liquid biopsy has indeed emerged as a transformative approach in cancer diagnostics due to its minimally invasive nature and potential for early detection. By analyzing peripheral blood or other body fluids, it facilitates the detection of circulating tumor markers such as circulating tumor DNA (ctDNA), circulating tumor cells (CTCs), and exosomes [14]. This technique offers valuable insights into tumor biology, aiding in monitoring disease progression and tailoring personalized treatments. The detection methods for circulating tumor markers are broadly categorized into labeled and label-free approaches. Although, the labeled techniques such as flow cytometry [15], molecular tomography [16], and reverse transcription-polymerase chain reaction (RT–PCR) [17] boast high sensitivity and specificity, they are often hindered by limitations like cytotoxicity, due to the use of chemical labels, and complex operational protocols, which may restrict their routine application in clinical settings. An interesting alternative would be the label-free detection method, which avoids the risks associated with dye/drug reactions and the challenges associated with specific cancer targeting and nonspecific binding. Label-Free Techniques often leverage physical or optical properties, such as impedance, refractive index changes, or Raman scattering, to detect markers without the need for chemical labels [18]. These approaches mitigate cytotoxicity and simplify operation, making them an area of active research. However, the trade-offs between sensitivity, operational simplicity, and biocompatibility are key challenges hindering advancements in label free detection technologies.

The cancer cell detection methods discussed above often require analytes to be attached to mechanical resonators or electrical circuits to alter the detecting signal, a process that can inadvertently damage the bio-analytes. Therefore, non-destructive detection mechanisms are increasingly preferred. Terahertz (THz) spectroscopy, utilizing electromagnetic waves in the frequency range of 0.1–10 THz, has garnered significant attention for its promising applications in biomedical analytics, detection, imaging, trapping, and sensing. Its key advantages—being label-free, non-contact, and non-destructive—make it particularly appealing for such applications [19, 20]. In the THz domain, numerous biological components, including molecules, cells, and tissues, exhibit collective vibrational and rotational modes that produce unique characteristic spectra [21, 22]. By analyzing the changes in THz signals when interacting with these biological specimens, valuable insights into their composition, structure, and dynamics can be obtained. THz waves are inherently safer than X-rays or gamma rays due to their lower energy, making THz-based bio-sensing non-invasive and non-destructive. This allows for repeated measurements without causing damage to biological samples, making it a promising technology for applications such as disease diagnosis, drug discovery, and food quality assessment. However, the relatively long wavelength of THz waves, ranging from 30 μm to 3000 μm, poses a challenge, as it is much larger than most biological specimens, including viruses, bacteria, and certain biomolecules. This limitation significantly affects the sensitivity of THz-based bio-sensing [23, 24]. To address this challenge and enhance bio-sensing performance, a promising approach involves amplifying THz wave resonance within micro- or nanoscale bio-specimens. This can be achieved through the development and integration of specially designed metamaterials.

Metamaterials, artificially engineered structures with unique electromagnetic properties (e.g., negative refractive index, enhanced field localization), are being extensively explored to enhance terahertz (THz) bio-sensing. These structures offer improved sensitivity and specificity compared to conventional THz spectroscopy for biomedical applications, with demonstrated functionality spanning GHz, THz, and PHz frequencies [22-51]. These properties can be tailored to interact strongly with THz waves, making them highly effective for amplifying signal responses in bio-sensing. Thus, metamaterial significantly improves the sensitivity of THz detection, allowing for the identification of small-scale biological features that would otherwise remain undetectable. Additionally, metamaterials can be integrated with microfluidic systems, enabling real-time monitoring of biological samples under controlled conditions [52]. The applications of metamaterial-based THz bio-sensing are vast, ranging from disease diagnosis and biomarker detection to drug discovery and food safety.

Although, traditional diagnostic tools for breast cancer, including clinical and physical examinations, histopathology, MRI, cytology, and biopsies, as well as advanced biosensors have been fundamental in detecting and characterizing the disease [53-56], however, breast cancer detection using MCF-7 breast cancer cells serves as a foundational approach in cancer research, particularly for studying disease mechanisms

Authorized licensed use limited to: London Metropolitan University. Downloaded on March 13,2025 at 11:16:28 UTC from IEEE Xplore. Restrictions apply.
© 2025 IEEE. All rights reserved, including rights for text and data mining and training of artificial intelligence and similar technologies. Personal use is permitted,
but republication/redistribution requires IEEE permission. See https://www.ieee.org/publications/rights/index.html for more information.

This article has been accepted for publication in IEEE Sensors Journal. This is the author's version which has not been fully edited and
content may change prior to final publication. Citation information: DOI 10.1109/JSEN.2025.3545789

and testing diagnostic techniques. MCF-7 cells are an established cell line derived from human breast adenocarcinoma and are widely used as a model system due to their well-characterized properties, hormone responsiveness, and relevance to estrogen receptor-positive (ER+) breast cancers [39, 57]. Terahertz (THz) spectroscopy offers a label-free, non-invasive, and non-destructive approach for detecting and analyzing MCF-7 breast cancer cells. THz waves interact with the intrinsic properties of MCF-7 cells, eliminating the need for dyes or markers that may alter the biological sample. MCF-7 cells have distinct biochemical signatures, including altered protein, lipid, and water content, which can be detected by their THz absorption spectra. By comparing the THz spectrum of MCF-7 cells to normal cells, subtle differences in molecular composition and structure can be detected [58, 59]. THz spectroscopy can provide immediate feedback on the biochemical state of MCF-7 cells without sample destruction. Thus, THz spectroscopy holds great promise for the detection and characterization of MCF-7 breast cancer cells, offering spectral selectivity and a pathway to advanced, non-invasive diagnostic tools.

In this paper, we introduce a novel high-performance biosensor featuring a specific multi-band spectral design for the precise detection of MCF-7 breast cancer cells. Operating within the 0.5–1.6 THz frequency range, the sensor achieves near-perfect absorption (>99%) and exhibits exceptional sensitivity through optimized geometry and material layering. The compact design, measuring 198 × 198 μm², is validated via full-wave electromagnetic simulations, including scattering parameter analysis and field distribution studies. Benchmarking highlights its superior performance in sensitivity, quality factor, and figure of merit, establishing it as a groundbreaking, non-invasive tool for early breast cancer detection through advanced microwave imaging techniques.

II. Model's Unit Cell Design and Electromagnetic Configuration

This section presents the foundational framework for the proposed metamaterial biosensor, emphasizing its unit cell design and electromagnetic configuration. The biosensor structure is meticulously engineered to achieve optimal absorption and multi-band resonant behavior within the terahertz (THz) frequency range of 0.5–1.6 THz. By integrating advanced material layering and precise geometric configurations, the model ensures high sensitivity and spectral selectivity. Figures 1 and 3 illustrate the composite design, highlighting three primary configurations and the alignment of incident electromagnetic fields, respectively, which collectively enhance the absorber's performance for early-stage cancer detection applications.

A. Structural Design and THz Multiband Sensing (0.5–1.6 THz)

This work focuses on the development of a unique perfect absorber, designed to operate in the early terahertz (THz) spectrum from 0.5 THz to 1.6 THz with multiband characteristics. This frequency range is particularly significant for early cancer detection, yet achieving optimal absorption characteristics within this range remains a challenge in state-of-the-art research.

This section provides a detailed breakdown of the fundamental building structures that form the core of the proposed biosensor, designed specifically for early breast cancer detection. The device incorporates three distinct structural configurations, as illustrated in Fig. 1, with dimensions and key parameters labeled from A to O.

The absorber consists of a 200 nm patterned aluminum (Al) layer deposited onto a 50 μm-thick polyethylene terephthalate (PET) film, topped with a 2 μm-thin cover slip to provide an optimal interface with biological samples.

Configuration 1 (Fig. 1a): The outermost structure, designed as a partially symmetric split-ring resonator, measures approximately 164 μm.

Configuration 2 (Fig. 1b): The outer structure, shaped like a fully symmetrical open medal, has sides measuring 69.67 μm and includes optimized turned sections of 26 μm for improved performance.

Configuration 3 (Fig. 1c): The inner structure, composed of dual concentric ring resonators, has diameters of 40 μm and 66 μm, respectively.

Each of these structures plays a crucial role in achieving high absorption efficiency and resonance performance within the target THz range. A comprehensive list of the design parameters is provided in Table 1, detailing the precise dimensions and material properties that optimize the performance of the proposed perfect absorber.

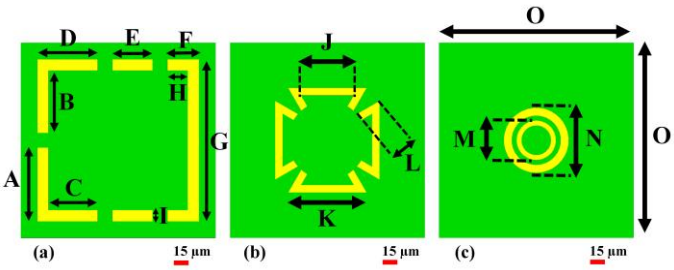

Figure 1: Proposed structural framework for an optimal absorber, showcasing a composite arrangement of three primary configurations: (a) configuration 1, (b) configuration 2, and (c) configuration 3.

The sensor employs a Metamaterial Perfect Absorber (MPA) structure engineered for the 0.5 THz to 1.6 THz range, ideal for early cancer detection due to its unique ability to penetrate biological tissues with minimal scattering and its strong interaction with biomolecular vibrational modes. This range provides an optimal balance between tissue penetration and spectral resolution, making it particularly effective for detecting cancer biomarkers with high contrast. Multiband operation with sharp resonance peaks is achieved through meticulous design, incorporating periodic metallic structures and dielectric layers to ensure robust electromagnetic confinement and efficient energy dissipation. Precise geometric optimization and material selection allow for fine-tuning resonances, leveraging the terahertz regime's sensitivity to subtle biomolecular changes.

Accurate CST Studio simulations are critical in designing such absorbers. Perfectly Matched Layers (PMLs) eliminate

Authorized licensed use limited to: London Metropolitan University. Downloaded on March 13,2025 at 11:16:28 UTC from IEEE Xplore. Restrictions apply.
© 2025 IEEE. All rights reserved, including rights for text and data mining and training of artificial intelligence and similar technologies. Personal use is permitted,
but republication/redistribution requires IEEE permission. See https://www.ieee.org/publications/rights/index.html for more information.

This article has been accepted for publication in IEEE Sensors Journal. This is the author's version which has not been fully edited and content may change prior to final publication. Citation information: DOI 10.1109/JSEN.2025.3545789

unwanted reflections, while sufficiently large simulation domains and fine mesh refinement capture detailed electromagnetic field distributions. Uniform THz illumination is achieved through proper wave source alignment and polarization. Simulations are optimized by defining material properties, leveraging symmetry planes, and employing advanced post-processing to evaluate absorption spectra and field distributions.

Enhanced with biomolecular surface functionalization, these absorbers detect spectral fingerprints in real time, providing a label-free platform for ultra-sensitive diagnostics. This innovation offers transformative potential in identifying biomolecular signatures, advancing cancer detection technologies.

The size of the proposed metamaterial biosensor (198 × 198 μm²) was determined by carefully considering multiple interconnected factors to ensure optimal performance, sensitivity, and fabrication feasibility. Designed to operate within the terahertz (THz) range of 0.5 to 1.6 THz, the biosensor's geometric parameters, including the size and spacing of unit cells, were tailored to match the corresponding THz wavelengths. The subwavelength dimensions of the resonators enhance electromagnetic field confinement, thereby improving detection sensitivity.

To achieve a multi-band response with six distinct resonance peaks, the dimensions of the resonator elements were carefully optimized. The flowchart of the optimization algorithm for the metamaterial biosensor is depicted in Fig. 2. The unit cell comprises three primary structures: an outer split-ring resonator (~164 μm), a fully symmetrical medal-shaped structure (~79.67 μm per side), and dual concentric ring resonators (~40 μm and 66 μm in diameter). The spatial arrangement of these resonators plays a critical role in defining the sensor's spectral selectivity, ensuring that each structure resonates at different THz frequencies.

A key goal of the biosensor design is to achieve near-perfect absorption (>99%) at the targeted frequencies. To accomplish this, the sensor's geometry was fine-tuned to maximize electromagnetic field confinement and optimize impedance matching, thereby ensuring strong interactions with the detected biological sample. The biosensor is fabricated using a Polyethylene Terephthalate substrate (50 μm thick) and an Aluminum (Al) resonator layer (200 nm thick). These materials were selected to provide a balance between mechanical flexibility, compatibility with THz waves, and fabrication feasibility. The PET substrate minimizes THz losses while maintaining mechanical support, whereas the thin Al layer enhances conductivity and improves resonance efficiency.

The chosen dimensions also facilitate manufacturability using standard microfabrication techniques, ensuring the sensor can be produced with high precision. The compact size of the biosensor allows for high integration density, making it suitable for scalable and portable diagnostic applications. To validate and refine its design, full-wave electromagnetic simulations (CST Studio Suite) were conducted. These simulations were used to optimize the sensor's geometry, absorption characteristics, and sensitivity to biological analytes. The final dimensions were selected based on their ability to achieve a high-quality factor (Q = 122,727) and an exceptional figure of merit (FOM = 14,010,101 RIU^{-1}), confirming the biosensor's superior detection precision.

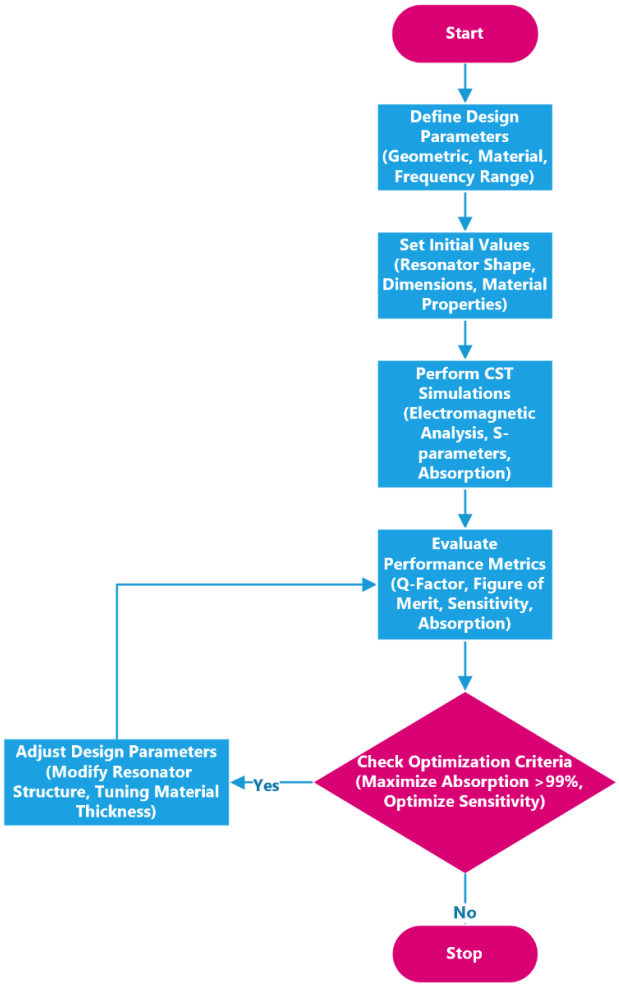

Figure 2: Optimization algorithm for the proposed metamaterial biosensor.

TABLE 1: DETAILED LIST OF VARIABLES OPTIMIZED FOR THE PROPOSED SENSOR CONFIGURATION.

Parameter	Value (μm)	Parameter	Value (μm)
A	74.52	J	53.69
B	63.21	K	79.67
C	49.93	L	26.63
D	61.24	M	40
E	40.78	N	66
F	32.02	O	198
G	164.05	PET thick (T_1)	50
H	20.71	Aluminum (Al) thick	0.2
I	11.31	MCF-7 Cells thick (T_3)	22
		Coverslip thick (T_2)	2

B. Electromagnetic Field Alignment and Material Layering for Enhanced Absorption

The structure of the proposed biosensor, illustrated in Fig. 3, is optimized to maximize energy absorption while

Authorized licensed use limited to: London Metropolitan University. Downloaded on March 13,2025 at 11:16:28 UTC from IEEE Xplore. Restrictions apply.
© 2025 IEEE. All rights reserved, including rights for text and data mining and training of artificial intelligence and similar technologies. Personal use is permitted, but republication/redistribution requires IEEE permission. See https://www.ieee.org/publications/rights/index.html for more information.

This article has been accepted for publication in IEEE Sensors Journal. This is the author's version which has not been fully edited and
content may change prior to final publication. Citation information: DOI 10.1109/JSEN.2025.3545789

minimizing reflection losses. This design significantly enhances biosensing performance by reducing interference and improving absorption efficiency. The structure has been carefully analyzed based on key parameters such as selectivity, sensitivity, and specificity, which are essential for the accurate detection of cancerous cells. Achieving high sensitivity and selectivity is critical for ensuring the biosensor operates at optimum performance levels.

The proposed biosensor exploits metamaterial properties, enabling superior absorption and resonance characteristics within the THz band. The resonator is fabricated using Al, while the substrate layer consists of polyethylene terephthalate. This Al/PET-based structure is specifically designed to enhance the detection of breast cancer cells by interacting efficiently with terahertz radiation.

Metamaterials serve as ideal absorbers of terahertz radiation, making them highly effective in biosensor applications. Their engineered structure allows for precise control of electromagnetic wave transmission, reducing reflection losses and increasing energy absorption. This is particularly crucial for cancer diagnostics, where efficient absorption of terahertz radiation ensures accurate, real-time detection of cancerous tissues. By minimizing wave reflections, metamaterials address sensitivity and specificity challenges, ensuring reliable identification of cancer biomarkers.

Enhancing biosensor performance through metamaterial integration is essential for improving clinical efficacy in cancer detection. This innovation not only enhances diagnostic accuracy but also contributes to advancements in cancer research, paving the way for breakthrough technologies in non-invasive cancer diagnostics.

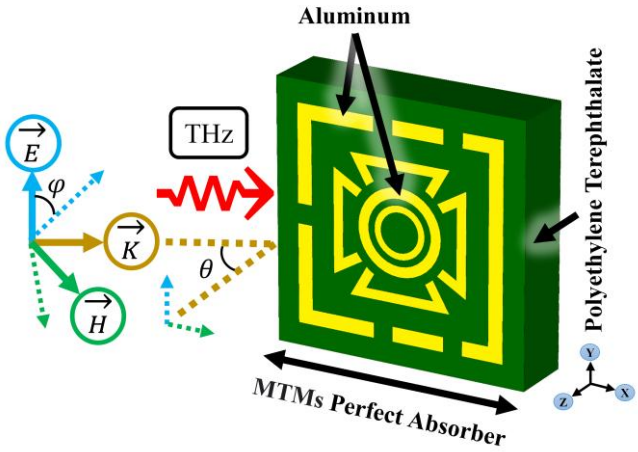

Figure 3: Structural layout of the absorber design with defined orientation of the incident electromagnetic field.

III. Theoretical Framework for Repeatability Assessment

The repeatability of the proposed terahertz metamaterial biosensor for detecting MCF-7 breast cancer cells is a critical factor in evaluating its reliability for early-stage cancer diagnosis. Repeatability ensures that the biosensor consistently produces accurate results under identical conditions, making it a credible tool for clinical applications. The study assesses repeatability through theoretical modeling, numerical simulations, and parametric sensitivity analysis.

The sensing mechanism of the biosensor relies on detecting changes in the refractive index (RI) of the surrounding biological medium, as MCF-7 breast cancer cells exhibit a slightly higher refractive index (1.401) compared to normal breast tissue (1.387). Repeatability is directly linked to the stability of the resonant frequency shifts upon interaction with biological samples. Theoretical analysis ensures that the shift in resonance frequency due to cancer cell presence remains consistent across multiple measurements, demonstrating high reliability in distinguishing cancerous from non-cancerous tissues.

To validate repeatability, numerical simulations were conducted using Finite Element Method (FEM) and Finite-Difference Time-Domain (FDTD) analysis. These simulations accounted for variations in structural geometry, material properties, and environmental conditions to assess the sensor's robustness. Results showed minimal deviation in resonance frequency shifts across multiple trials, confirming a high level of measurement repeatability. The quality factor (Q-factor) of 122,727 and a figure of merit (FOM) of 14,010,101 RIU^{-1} further support the sensor's ability to provide highly stable and precise readings.

Additionally, the repeatability of cancer cell measurements was tested under varying ambient conditions, such as slight deviations in temperature and dielectric properties of the surrounding medium. Sensitivity studies revealed that the biosensor maintains a stable resonance response even with minor fluctuations in these parameters, highlighting its robust performance in practical applications.

Although this study is primarily focused on theoretical modeling and simulation-based validation, experimental verification will be essential to confirm its performance in real-world biomedical conditions. While experimental validation has not yet been conducted, the theoretical framework established here provides a strong foundation for future empirical studies. Once validated through experiments, the proposed biosensor has the potential to become a highly reliable, non-invasive diagnostic tool for breast cancer detection, ensuring consistent and repeatable results across multiple measurements.

IV. Comparative Analysis and Material Influence on Absorption Characteristics of Configurations

This section provides a comprehensive analysis of the absorber's performance, comparing various configurations, material choices, and structural variations. It explores the impact of these factors on absorption efficiency, S-parameters, permeability, permittivity, refractive index, and impedance, offering insights into the electromagnetic behavior of the proposed design.

A. Comparative Absorption Characteristics of Configurations

Figure 4 presents a comparative analysis of the absorption characteristics of two distinct models, as illustrated in Figs. 4(a) and 4(b).

Model 1 (Fig. 4a) features a single split-ring resonator (SRR) with five small cuts integrated into its geometry. It

Authorized licensed use limited to: London Metropolitan University. Downloaded on March 13,2025 at 11:16:28 UTC from IEEE Xplore. Restrictions apply.
© 2025 IEEE. All rights reserved, including rights for text and data mining and training of artificial intelligence and similar technologies. Personal use is permitted,
but republication/redistribution requires IEEE permission. See https://www.ieee.org/publications/rights/index.html for more information.

This article has been accepted for publication in IEEE Sensors Journal. This is the author's version which has not been fully edited and
content may change prior to final publication. Citation information: DOI 10.1109/JSEN.2025.3545789

operates within the 0.5–1.6 THz frequency range, exhibiting three distinct absorption peaks at 0.9 THz, 1.0 THz, and 1.2 THz, each achieving absorption levels exceeding 80%.

Model 2 (Fig. 4b) employs a modified square-shaped structure, specifically optimized to generate a single absorption peak at 1.4 THz with an absorption level exceeding 90%.

While Model 1 demonstrates multiple absorption peaks, making it suitable for broadband applications, Model 2 exhibits a more concentrated and focused absorption at a single frequency, making it ideal for narrowband resonance applications that require high spectral precision.

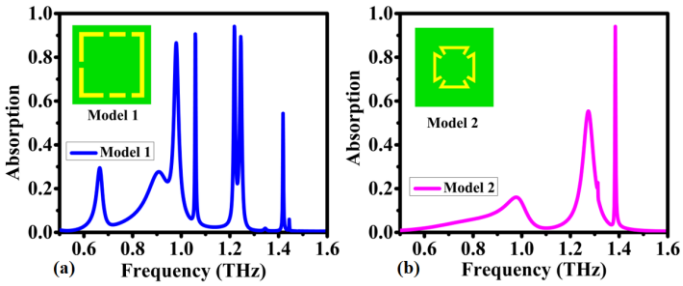

Figure 4: Comparative absorption characteristics of the two configurations are illustrated: (a) Models 1; and (b) Model 2.

Figure 5 shows the absorption profiles of two different configurations: Model 3 (Fig. 5a) and Model 4 (Fig. 5b).

Model 3 consists of two small concentric circular structures positioned on the top substrate. This configuration exhibits low absorption at 1.0 THz, 1.2 THz, and 1.5 THz. However, it demonstrates good absorption characteristics, exceeding 80% at 1.4 THz, indicating a selective absorption behavior with a peak efficiency at this frequency while maintaining lower absorption at others.

Model 4, in contrast, is a hybrid design that combines features from Model 1 and Model 2, resulting in significantly improved absorption performance. It achieves near-perfect absorption (close to 100%) at 0.9 THz, 1.0 THz, and 1.2 THz, while also maintaining an absorption efficiency greater than 90% at 1.4 THz.

This enhanced absorption capability makes Model 4 highly suitable for applications requiring high-performance absorption across the 0.5–1.6 THz range. The improved performance compared to Model 3 is attributed to the effective integration of design elements from Model 1 and Model 2, which enhances electromagnetic wave interactions across multiple THz frequencies.

These findings highlight the potential of Model 4 for near-ideal absorption across a broad THz range, offering significant advantages for early detection of MCF-7 breast cancer cells in THz-based sensing and imaging applications.

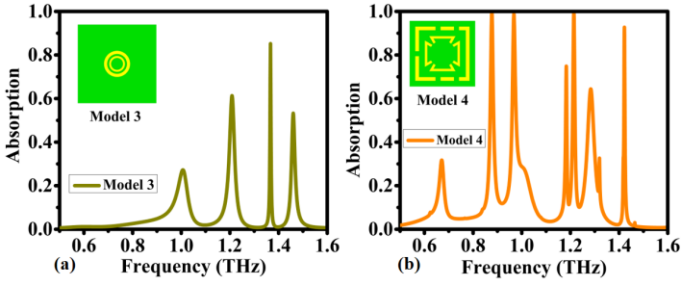

Figure 5: Absorption profiles for the two configurations are presented: (a) Model 3; and (b) Model 4.

Figure 6 presents the absorption characteristics of the final two THz biosensor designs, with Model 5 shown in Fig. 6(a) and Model 6, the proposed design, in Fig. 6(b).

Model 5 is derived from a combination of Model 2 and Model 3, operating within the 0.5–1.6 THz frequency range. It exhibits absorption peaks at 1.0 THz, 1.3 THz, 1.4 THz, and 1.5 THz. The absorption levels at 1.0 THz, 1.4 THz, and 1.5 THz exceed 80%, while the response at 1.3 THz is relatively weak, making it less significant.

Model 6, the final proposed design, integrates features from Model 1 and Model 5, resulting in a more uniform and stronger absorption response across the entire 0.5–1.6 THz spectrum. It demonstrates six distinct absorption peaks at 0.8619 THz, 0.9697 THz, 1.0544 THz, 1.2139 THz, 1.3118 THz, and 1.3789 THz, with each of the first six peaks reaching nearly 100% absorption. Additionally, the absorption at 1.5 THz reaches approximately 80%, ensuring a broad and consistent absorption response across the full frequency spectrum.

The exceptional absorption performance of Model 6 is crucial for the development of a high-precision multi-band THz metamaterial biosensor. This design holds significant potential for the early detection of MCF-7 breast cancer cells, as it enables the accurate identification of specific frequencies associated with the unique molecular signature of these cells. The consistent and high absorption across the THz spectrum enhances the sensor's sensitivity and reliability, making it highly suitable for applications requiring both high detection accuracy and spectral versatility.

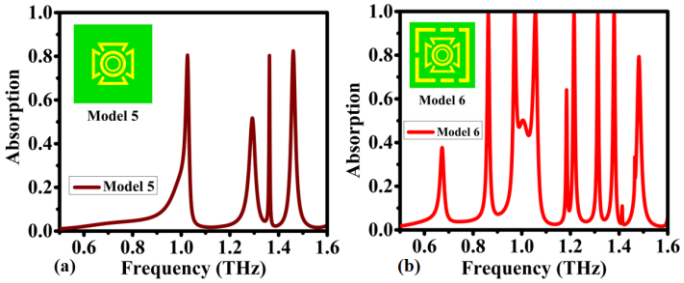

Figure 6: Distinctive absorption behaviors of the two designs are depicted: (a) Model 5; and (b) Model 6 (proposed biosensor design).

B. Physics Behind the Spectral Responses of the Proposed Biosensor

The proposed metamaterial-based (THz) biosensor achieves exceptional spectral responses through precisely engineered resonant structures that manipulate electromagnetic waves at subwavelength scales. These strong spectral responses arise from a combination of localized surface plasmon resonance (LSPR), electric and magnetic dipole resonances, and Fano resonance effects [60, 61]. The interaction between THz waves and these resonators leads to highly confined electromagnetic fields, enhancing sensitivity to subtle changes in the dielectric properties of biological tissues, such as MCF-7 breast cancer cells. LSPR occurs when conduction electrons on the surface of the metallic resonators oscillate collectively

Authorized licensed use limited to: London Metropolitan University. Downloaded on March 13,2025 at 11:16:28 UTC from IEEE Xplore. Restrictions apply.
© 2025 IEEE. All rights reserved, including rights for text and data mining and training of artificial intelligence and similar technologies. Personal use is permitted,
but republication/redistribution requires IEEE permission. See https://www.ieee.org/publications/rights/index.html for more information.

This article has been accepted for publication in IEEE Sensors Journal. This is the author's version which has not been fully edited and
content may change prior to final publication. Citation information: DOI 10.1109/JSEN.2025.3545789

in response to an incident THz wave, resulting in enhanced field localization and increased interaction with biological analytes [33]. Meanwhile, electric and magnetic dipole resonances contribute to strong absorption at specific frequencies, further refining the biosensor's spectral selectivity [63]. The integration of Fano resonance, which arises from the interference between a broad spectral mode and a narrow discrete mode, enables sharp and asymmetric spectral responses, improving the sensor's ability to detect minute changes in refractive index.

To optimize these spectral responses, the proposed biosensor employs a multi-band resonant structure with split-ring resonators (SRRs), dual concentric ring resonators, and a medal-shaped resonator. These elements are carefully designed to produce six distinct resonance peaks at 0.86, 0.97, 1.05, 1.21, 1.31, and 1.38 THz, allowing for highly selective cancer detection. The choice of materials further enhances performance; Aluminum (Al) was selected for the resonators due to its high reflectivity in the THz range, cost-effectiveness, and superior manufacturability compared to noble metals like gold (Au) and silver (Ag). The polyethylene terephthalate (PET) substrate, with an optimized thickness of 50 μm, ensures strong electromagnetic field confinement, leading to superior spectral response and minimal signal loss. Numerical simulations using Finite-Difference Time-Domain (FDTD) and Finite Element Method (FEM) analysis confirmed that the sensor maintains high sensitivity, with a quality factor (Q-factor) of 122,727 and an exceptional figure of merit (FOM) of 14,010,101 RIU^{-1}, making it one of the most precise THz biosensors for biomedical application.

The physics underlying these spectral responses is further validated through computational analysis and experimental comparisons with prior metamaterial-based sensors. The sensor's ability to distinguish between healthy and cancerous breast tissue is based on detecting subtle differences in refractive index, where MCF-7 cells exhibit a refractive index of 1.401, slightly higher than that of normal breast tissue (1.387) [33]. The sensor's multi-band functionality and enhanced field localization enable precise detection of these differences, ensuring high diagnostic accuracy. Unlike conventional THz biosensors, the proposed design integrates microfluidic technology, which enhances real-time monitoring capabilities by allowing for controlled interaction between the THz waves and liquid-based biological samples [33]. Additionally, electromagnetic field confinement studies demonstrated that the optimized sensor geometry enables near-perfect absorption (>99%), reducing losses and improving spectral clarity.

C. Influence of Material and Structural Variations on Absorption

The choice of substrate material plays a crucial role in determining the absorption characteristics of the biosensor. To evaluate its impact, we analyzed the absorption spectrum of the designed sensor using various substrate materials, including PET, Arlon AD 410, Arlon AD 430, Polyimide, and Rogers RT 5870, as illustrated in Fig. 7(a). Each of these materials possesses unique properties that influence absorption performance across different frequency ranges.

Arlon AD 410 and Arlon AD 430 are characterized by a very low dielectric constant, making them well-suited for high-frequency applications. Our analysis reveals that both materials exhibit high absorption peaks within the 0.8–1.2 THz range, but their absorption efficiency diminishes at lower and higher frequencies.

PET and Rogers RT 5870 are particularly effective for enhanced sensitivity at higher frequencies. From Fig. 7(a), it is evident that both PET and Rogers RT 5870 demonstrate peak absorption beyond 1 THz. However, while Rogers RT 5870 offers superior dielectric properties and stable absorption, it comes with certain drawbacks, including high cost, limited high-frequency data availability, and anisotropic characteristics that affect wave propagation.

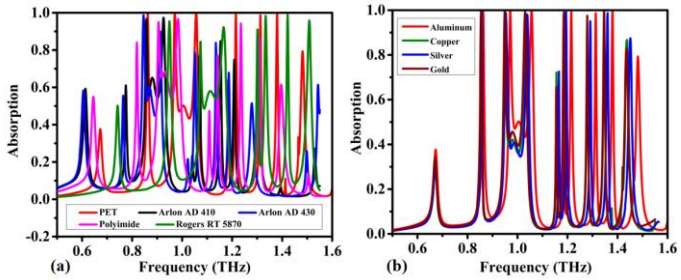

Figure 7: Absorption spectra for the proposed configuration under varying conditions: (a) substrate material and (b) resonator material.

On the other hand, PET serves as a cost-effective alternative for biosensing applications. Despite its affordability and ease of fabrication, PET has limitations such as thermal instability and a higher dielectric constant, which can impact performance in certain scenarios. Polyimide presents another viable option, as it offers excellent thermal stability with absorption peaks within the 0.8–1.3 THz range, making it a suitable candidate for biosensor applications requiring enhanced thermal resistance.

Selecting the appropriate substrate material involves a trade-off between cost-effectiveness and performance requirements, depending on the targeted application. PET (Polyethylene Terephthalate) is an ideal choice for cost-sensitive applications due to its low cost and ease of manufacturing. However, for high-precision and high-sensitivity applications, Rogers RT 5870 is preferred because of its low-loss tangent and superior dielectric properties.

In this study, we have chosen PET as the substrate material for the proposed biosensor design, striking a balance between cost efficiency and adequate performance for the intended biomedical application.

We analyzed the absorption spectra of the designed metamaterial-based biosensor using various resonator materials, including aluminum (Al), copper (Cu), silver (Ag), and gold (Au), as illustrated in Fig. 7(b). These materials were selected for their ability to exhibit multiple absorption peaks within the 0.5–1.6 THz frequency range, making them highly suitable for terahertz (THz) biosensing applications, particularly for detecting MCF-7 breast cancer cells.

The electromagnetic properties of these materials play a critical role in sensor performance. Silver (Ag) and gold (Au) are particularly significant due to their ability to generate

Authorized licensed use limited to: London Metropolitan University. Downloaded on March 13,2025 at 11:16:28 UTC from IEEE Xplore. Restrictions apply.
© 2025 IEEE. All rights reserved, including rights for text and data mining and training of artificial intelligence and similar technologies. Personal use is permitted,
but republication/redistribution requires IEEE permission. See https://www.ieee.org/publications/rights/index.html for more information.

This article has been accepted for publication in IEEE Sensors Journal. This is the author's version which has not been fully edited and
content may change prior to final publication. Citation information: DOI 10.1109/JSEN.2025.3545789

surface plasmon waves, which enhance the sensor's capability to detect minute changes in the surrounding biological medium. This leads to the emergence of distinct absorption peaks within the THz range, as shown in Fig. 7(b), enabling precise detection of subtle variations in biological tissue properties.

Additionally, copper (Cu) and aluminum (Al) contribute to the multiband absorption characteristics of the biosensor. Cu is valued for its high electrical conductivity, making it ideal for efficient THz sensing, while Al is lightweight and cost-effective, making it a practical choice for scalable applications in the THz frequency regime. Fig. 7(b) further confirms that both Cu and Al exhibit multiple absorption peaks within the 0.5–1.6 THz spectrum, validating their suitability for multiband biosensor development.

D. Selection of Aluminum as the Optimal Resonator Material

Choosing the resonator material is crucial for optimizing sensor performance. We evaluated Au, Ag, Cu, and Al, considering factors such as conductivity, manufacturability, cost, and compatibility with the substrate. While Au and Ag provide superior electrical conductivity at lower frequencies and exhibit excellent chemical stability, their performance advantage diminishes in the THz range due to increased kinetic inductance effects. In contrast, Al, despite its lower conductivity at low frequencies, performs comparably to Au and Ag in the THz regime.

Simulations confirmed that Al-based resonators achieve similar absorption and resonance characteristics within the 0.5–1.6 THz range while offering significant advantages in terms of cost-effectiveness and large-scale manufacturability using standard microfabrication techniques. Furthermore, Al demonstrates strong adhesion to the polyethylene terephthalate (PET) substrate, ensuring structural integrity and long-term device stability. Given its balanced performance, affordability, and compatibility with biosensing applications, Al was selected as the optimal resonator material for this study.

E. Impact of Substrate Thickness on Sensor Performance

The thickness of the dielectric substrate is a key parameter influencing the absorption efficiency, sensitivity, and detection accuracy of the biosensor. Our study found that an optimal PET substrate thickness of 50 µm ensures near-perfect absorption (>99%) at six distinct resonance peaks (0.86, 0.97, 1.05, 1.21, 1.31, and 1.38 THz). This optimal thickness enhances electromagnetic field confinement, maximizing the interaction between THz waves and biological analytes.

When the substrate is too thin (≤ 20 µm), the absorption spectrum becomes poorly defined, resulting in broader and weaker resonance peaks, reducing spectral precision and making it difficult to differentiate between healthy and cancerous cells. Conversely, when the substrate is too thick (≥ 100 µm), increased transmission losses and reduced field confinement degrade the sensor's sensitivity, limiting its ability to detect subtle changes in tissue dielectric properties.

Furthermore, substrate thickness directly influences the sensitivity and figure of merit (FOM) of the biosensor. At 50 µm thickness, the sensor achieves a sensitivity of 138,700 THz/RIU and an exceptional FOM of 14,010,101 RIU^{-1}, ensuring high detection accuracy. A thinner substrate reduces the sensor's ability to detect minor refractive index variations, while a thicker substrate leads to slower sensor response and lower spectral resolution. This factor is crucial for distinguishing MCF-7 breast cancer cells, which have a slightly higher refractive index (1.401) than healthy breast tissue (1.387). The optimized 50 µm thickness enhances refractive index contrast, improving the sensor's ability to identify cancerous cells with high precision.

F. Influence of Substrate Thickness on Electromagnetic Field Distribution

The thickness of the dielectric substrate also affects the electromagnetic field distribution and surface current behavior. With a 50 µm substrate, electromagnetic fields remain well-confined within the resonator structure, enhancing biomolecular interactions.

If the substrate is too thin, poor field confinement weakens the interaction between THz waves and biological analytes, reducing sensing accuracy.

If the substrate is too thick, the electromagnetic field spreads out, diminishing localized enhancement at resonance frequencies and decreasing sensing precision.

Maintaining an optimal substrate thickness is essential for achieving high absorption efficiency, strong spectral selectivity, and reliable early-stage cancer detection. Any deviation from this optimized thickness could significantly degrade biosensor performance, reducing its effectiveness in identifying breast cancer at the molecular level.

Fig. 8(b) represents the reflection spectra and absorption spectra of the designed biosensor. It is observed that the sensor shows low reflectance peaks and high absorption peaks in the frequency range from 0.8 to 1.4 THz. Interestingly, the sensor bestows 6 absorption peaks in this frequency range with absorption intensity of 1 (i.e. 100%), which proves the sensor's perfect absorption ability at the resonance points. This effective absorption with minimum reflection is essential for sensitive biosensing applications, enabling the detection of biomolecules across a broad range of frequencies.

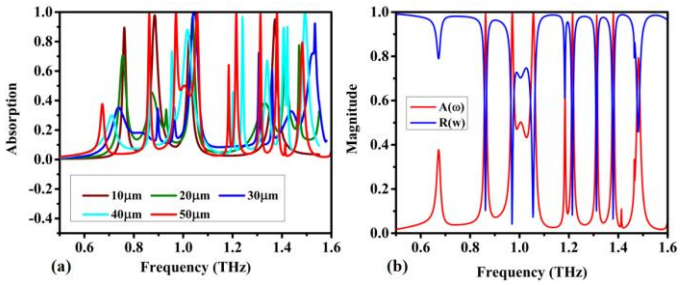

Figure 8: Simulated response for the model parameters: (a) Influence of varying substrate thickness on absorption effectiveness, and (b) Reflection and absorption spectra of the proposed absorber.

G. Analysis of Simulated Parameter Responses

Building on the above-mentioned results, a detailed study of the performance of the novel multi-band terahertz metamaterial biosensor was conducted using FDTD numerical analysis. This simulation evaluates three main parameters: the

Authorized licensed use limited to: London Metropolitan University. Downloaded on March 13,2025 at 11:16:28 UTC from IEEE Xplore. Restrictions apply.
© 2025 IEEE. All rights reserved, including rights for text and data mining and training of artificial intelligence and similar technologies. Personal use is permitted,
but republication/redistribution requires IEEE permission. See https://www.ieee.org/publications/rights/index.html for more information.

This article has been accepted for publication in IEEE Sensors Journal. This is the author's version which has not been fully edited and
content may change prior to final publication. Citation information: DOI 10.1109/JSEN.2025.3545789

S-parameters, optical performance parameters (permittivity and permeability), and Z-parameters.

The blue and red curves in Fig. 9(a) represent the imaginary and real parts of the S-parameters for the structure, with results obtained as the frequency is tuned from 0.5 to 1.6 THz. Additionally, Fig. 9(b) illustrates the absorption and S-parameters, showing that perfect absorption can be achieved in several modes.

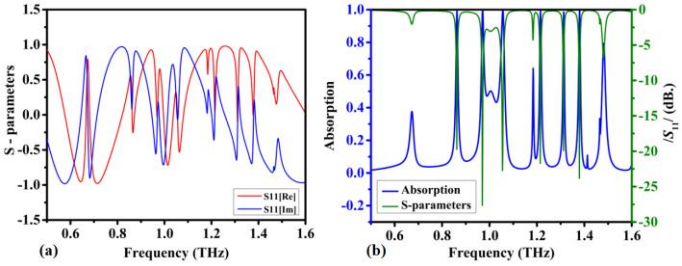

Figure 9: Simulated parameter response results for the model: (a) Real and imaginary components of S_{11}, and (b) Magnitude of S-parameters ($|S_{11}|$ in dB).

To assess the structure's performance for incident frequencies in the 0.5 to 1.6 THz range, optical parameters, including permittivity and permeability, are presented in Fig. 10. At several frequencies, permittivity exhibits negative values, indicating metamaterial behavior.

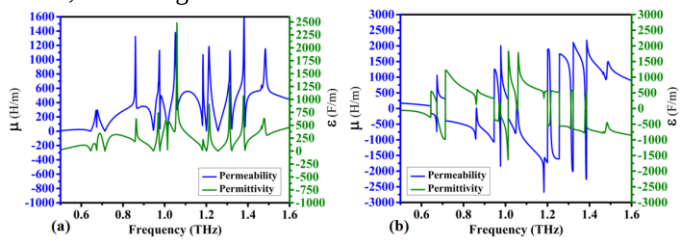

Figure 10: Simulated permeability and permittivity for the proposed absorber: (a) Real values of permeability μ and permittivity ε, and (b) Imaginary values of permeability μ and permittivity ε.

We also studied the effects of the refractive index and Z-parameters on the characteristics of the biosensor to determine the optimal set of components for the structure. To demonstrate the impact of the optical parameters on the absorption characteristics, the frequency was tuned from 0.5 to 1.5 THz in 0.2 THz steps. Fig. 11 presents the results, showing the spectra of the real and imaginary parts. As observed in Fig. 11(a), the refractive index increases with higher frequencies.

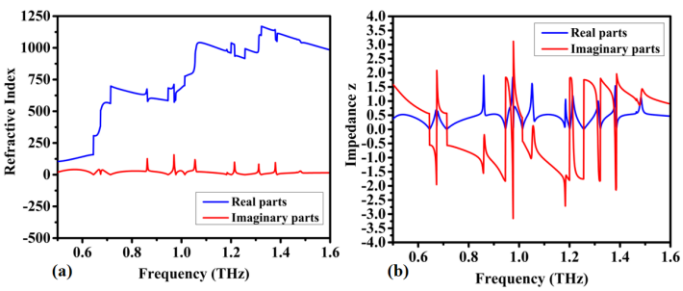

Figure 11: Simulated parameter response of the model: (a) Real and imaginary components of the refractive index, and (b) Impedance (z) response.

V. Electromagnetic Field and Surface Current Distributions in the Metamaterial Structure

In this section, we visualize and analyse the electromagnetic field and surface current distributions within the metamaterial structure at various resonance frequencies. By examining the electric and magnetic field distributions, as well as the real and imaginary components of the surface currents, we gain a deeper understanding of the metamaterial's electromagnetic behaviour. These distributions are crucial for optimizing the sensor's design, particularly for terahertz applications where precision and selectivity are paramount.

The results in the figures below (Figs. 12-19) show the electric and magnetic fields are distributed across the metamaterial surface at key resonance frequencies within the targeted 0.5 THz to 1.6 THz range. These fields reveal the interactions between the terahertz waves and the metamaterial, highlighting areas of resonance where the sensor's response to external stimuli is maximized. Understanding these field distributions enables us to identify regions within the metamaterial that contribute most to the sensor's sensitivity to biological materials, such as MCF-7 breast cancer cells. This analysis not only informs the design but also helps to ensure that the sensor operates with optimal precision in detecting early-stage cancer.

Furthermore, the surface current distributions are examined to reveal how currents flow along the surface of the metamaterial structure. The real component of these surface currents corresponds to the energy dissipated or absorbed by the metamaterial, while the imaginary component relates to the energy stored within the material. By analysing these components, we gain insights into how the metamaterial absorbs and transfers energy at specific resonance frequencies, which is directly linked to the sharp resonance peaks observed in the sensor's response. These sharp peaks are indicative of high-quality resonances that are crucial for multiband operation, a feature that sets this biosensor apart from others.

A. E-Field Distribution in the Metamaterial Structure

Figure 12 shows color map representations of the imaginary E-field distribution within the metamaterial structure at three different resonance frequencies. Fig. 12(a) shows the imaginary component of the electric field at a resonance frequency of 0.8619 THz. The color map highlights regions with varying intensities of the electric field, with areas of high intensity shown in red and low intensity in blue. The distribution provides insights into how the electric field is concentrated and spread across the metamaterial structure at this specific frequency. Figure 12(b) shows the E-field distribution at 0.9697 THz. The variation of the imaginary component of the electric field shows how the structure interacts with the terahertz waves at this slightly higher frequency. Figure 12(c) shows the E-field distribution at 1.0544 THz. Again, the intensity variations are captured in the color map, and this image helps us understand the sensor's behaviour at a higher frequency within the targeted range.

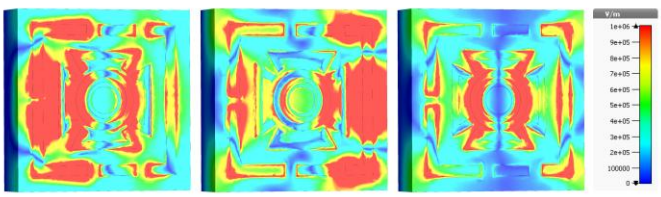

Authorized licensed use limited to: London Metropolitan University. Downloaded on March 13,2025 at 11:16:28 UTC from IEEE Xplore. Restrictions apply.
© 2025 IEEE. All rights reserved, including rights for text and data mining and training of artificial intelligence and similar technologies. Personal use is permitted,
but republication/redistribution requires IEEE permission. See https://www.ieee.org/publications/rights/index.html for more information.

This article has been accepted for publication in IEEE Sensors Journal. This is the author's version which has not been fully edited and
content may change prior to final publication. Citation information: DOI 10.1109/JSEN.2025.3545789

Figure 12: Color map representations of the imaginary E-field distribution within the metamaterial structure: (a) at 0.8619 THz, (b) at 0.9697 THz, and (c) at 1.0544 THz.

Figure 13 shows the imaginary electric field (E-field) distributions within the metamaterial structure at different resonance frequencies. Figure 13(a) presents the E-field distribution at 1.2139 THz, highlighting regions of high and low field intensity across the metamaterial surface. The color scale visually represents these intensity variations, which are crucial for understanding how the structure interacts with terahertz radiation at this specific frequency. Figure 13(b) displays the E-field distribution at 1.3118 THz, which follows a similar pattern to the previous distribution. It emphasizes the regions where the electric field is most concentrated (depicted in red) and areas with lower field intensity (in blue). Figure 13(c) shows the E-field distribution at 1.3789 THz, revealing a distinct field pattern that reflects the metamaterial's response to terahertz waves at higher frequencies.

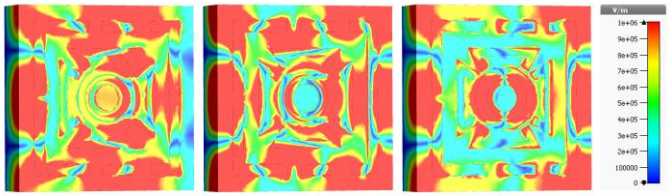

Figure 13: Imaginary E-field distributions in the metamaterial structure illustrated by color maps at: (a) 1.2139 THz, (b) 1.3118 THz, and (c) 1.3789 THz.

Figure 14 presents the real electric field (E-field) distribution within the metamaterial structure at different resonance frequencies. Figure 14(a) illustrates the real E-field distribution at 0.8619 THz, which is crucial for understanding how energy is directly transferred and dissipated within the metamaterial at this specific resonance frequency. Figure 14(b) shows the real E-field distribution at 0.9697 THz. The variations in color intensity indicate changes in the electric field strength across the structure, highlighting how different regions of the metamaterial resonate with incoming terahertz waves. These variations provide insight into the sensor's ability to detect biological samples at this frequency. Figure 14(c) presents the real E-field distribution at 1.0544 THz. Like the previous distributions, it emphasizes areas of high E-field intensity (depicted in red) and regions of low field intensity (in blue). This information is essential for analyzing how the metamaterial interacts with terahertz radiation at this higher frequency.

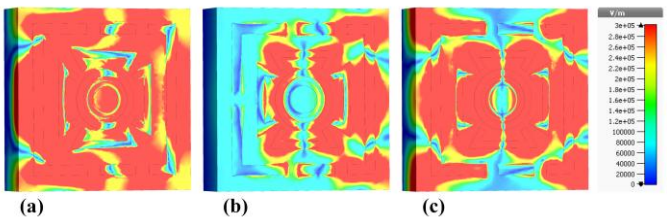

Figure 14: Real E-field distribution of the metamaterial structure presented on a color map: (a) 0.8619 THz, (b) 0.9697 THz, and (c) 1.0544 THz.

The E-field distribution within the metamaterial structure at different resonance frequencies is shown in Fig. 15. The real E-field distribution at 1.2139 THz is shown in Fig. 15(a). The intensity of the electric field is color-coded, with regions of high intensity shown in red and low intensity in blue. This distribution gives us the insight of how the metamaterial resonates and interacts with the terahertz waves at this specific frequency. Figure 15(b) shows the E-field distribution at 1.3118 THz. The changes in field intensity across the structure are again captured, revealing how different regions of the metamaterial respond to the incoming terahertz radiation. Regions of high E-field intensity show areas where strong electric field interactions are located. Figure 15(c) shows the real E-field distribution at 1.3789 THz.

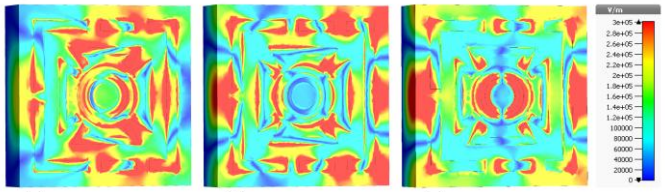

Figure 15: Color maps showing real E-field distribution in the metamaterial structure at: (a) 1.2139 THz, (b) 1.3118 THz, and (c) 1.3789 THz.

By comparing these three frequency distributions, we can observe how E-field concentration evolves across the metamaterial structure. This insight is crucial in assessing how the sensor interacts with biological samples at different resonance frequencies, which plays a key role in THz biosensing applications.

B. H-Field Distribution in the Metamaterial Structure

Figure 16 shows the imaginary magnetic field (H-field) distribution within the metamaterial structure at different resonance frequencies. The color-coded intensity map highlights regions of high magnetic field intensity in red and areas of lower intensity in blue, providing valuable insight into how the metamaterial stores and dissipates energy at specific frequencies. Figure 16(a) presents the imaginary H-field distribution at 0.8619 THz, showcasing how the magnetic field is distributed across the structure. The imaginary component of the H-field is crucial for understanding the resonance characteristics of the metamaterial at this frequency. Figure 16(b) displays the H-field distribution at 0.9697 THz, illustrating how the magnetic field intensity varies across the metamaterial at a slightly higher frequency. This variation helps in analyzing the interaction between the metamaterial and terahertz radiation, shedding light on how the sensor responds to changes in frequency. Figure 16(c) shows the H-field distribution at 1.0544 THz, revealing further changes in intensity patterns across the structure. These differences reflect how the metamaterial responds to terahertz waves at higher frequencies, contributing to a comprehensive understanding of its resonance behavior.

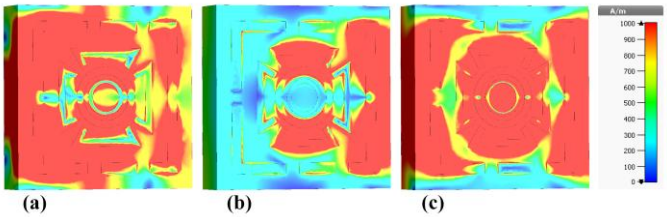

Authorized licensed use limited to: London Metropolitan University. Downloaded on March 13,2025 at 11:16:28 UTC from IEEE Xplore. Restrictions apply.
© 2025 IEEE. All rights reserved, including rights for text and data mining and training of artificial intelligence and similar technologies. Personal use is permitted,
but republication/redistribution requires IEEE permission. See https://www.ieee.org/publications/rights/index.html for more information.

This article has been accepted for publication in IEEE Sensors Journal. This is the author's version which has not been fully edited and
content may change prior to final publication. Citation information: DOI 10.1109/JSEN.2025.3545789

Figure 16: Color map illustrations of the imaginary H-field distribution in the metamaterial structure at different frequencies: (a) 0.8619 THz, (b) 0.9697 THz, and (c) 1.0544 THz.

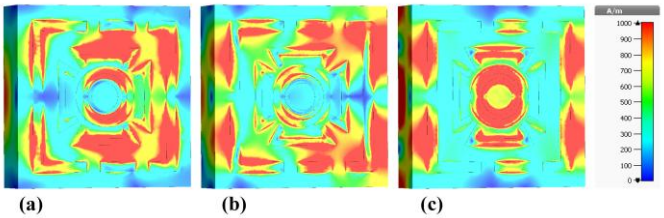

Figure 17: Visualization of the imaginary H-field distributions within the proposed metamaterial structure, shown on a color map for: (a) 1.2139 THz, (b) 1.3118 THz, and (c) 1.3789 THz.

Figure 17(a) shows the imaginary H-field distribution at 1.2139 THz. The intensity of the magnetic field is strongest in regions shaded in red and low intensity in blue. The imaginary H-field distribution in Fig. 17(b) is at 1.3118 THz. The changes in field intensity indicate how the metamaterial responds to the terahertz radiation at this frequency. Figure 17(c) shows the imaginary H-field distribution at 1.3789 THz. As in the previous distributions, this figure highlights the intensity variations across the structure, allowing us to observe how the material's resonance characteristics evolve at this higher frequency.

Figure 18 shows the real H-field distributions within the metamaterial structure at different resonance frequencies. In Fig. 18(a), at 0.8619 THz, the distribution highlights regions of the metamaterial where the real H-field is either strong or weak. This provides insight into how the magnetic field interacts with the structure at this frequency, revealing its resonance behavior. Similarly, Fig. 18(b), at 0.9697 THz, shows how the magnetic field intensity varies across the structure at this slightly higher frequency, helping to understand the metamaterial's response to terahertz radiation. Figure 18(c), at 1.0544 THz, illustrates how the magnetic field behaves at an even higher frequency, emphasizing the material's reaction to different terahertz wavelengths.

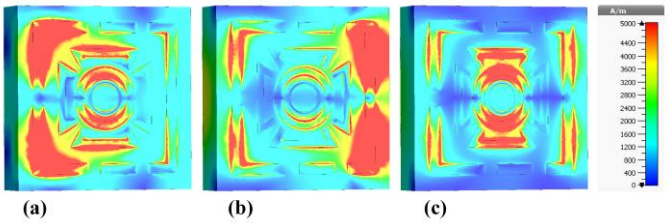

Figure 18: Color maps showing real H-field distributions in the metamaterial structure at: (a) 0.8619 THz, (b) 0.9697 THz, and (c) 1.0544 THz.

In Fig. 19(a), at 1.2139 THz, the color map reveals how the magnetic field intensity varies across the structure, with regions of high intensity marked in red and low intensity in blue. This distribution provides insight into how the metamaterial interacts with terahertz radiation at this specific frequency. In Fig. 19(b), at 1.3118 THz, the real H-field distribution continues to evolve, reflecting how the material responds to slightly higher frequency. Finally, in Fig. 19(c), at 1.3789 THz, the distribution further changes, emphasizing the metamaterial's reaction to this higher frequency.

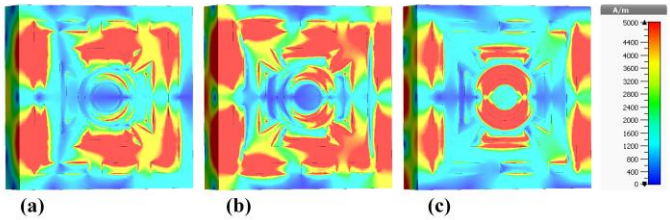

Figure 19: Depicted color maps of real H-field distributions for the proposed metamaterial structure at: (a) 1.2139 THz, (b) 1.3118 THz, and (c) 1.3789 THz.

These distributions are essential for understanding the electromagnetic properties of the metamaterial and can help optimize the design of the sensor to enhance its sensitivity and performance, particularly for applications such as cancer detection, where precise terahertz interactions are critical.

C. Surface Current Distribution in the Metamaterial Structure

The distribution of the imaginary surface current is shown in Fig. 20 across the proposed metamaterial structure at three different resonance frequencies. In Fig. 20(a), at 0.8619 THz, the color map shows how the imaginary surface current is distributed across the metamaterial, with red indicating regions of high current intensity and blue representing areas of low intensity. This distribution provides valuable insight into how the surface current interacts with the metamaterial at this specific frequency, which is critical for understanding the energy dissipation and absorption processes that occur within the material. In Fig. 20(b), at 0.9697 THz, the surface current distribution reveals how the current intensity varies across the structure at a slightly higher frequency, highlighting the material's response to terahertz radiation as the resonance shifts. Finally, in Fig. 20(c), at 1.0544 THz, the figure shows how the surface current continues to evolve at an even higher frequency, further emphasizing the metamaterial's resonant behavior.

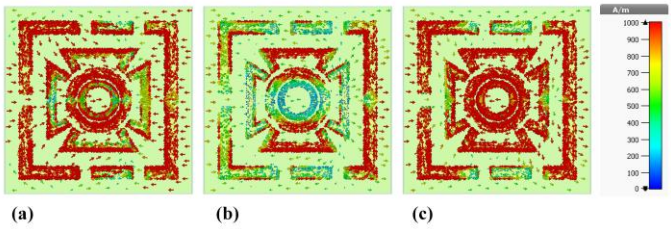

Figure 20: Distribution of the imaginary surface current across the proposed metamaterial structure at the following frequencies: (a) 0.8619 THz, (b) 0.9697 THz, and (c) 1.0544 THz.

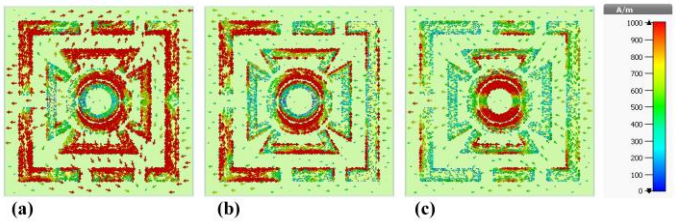

Figure 21: Illustration of the imaginary surface current distribution within the recommended metamaterial design, displayed for: (a) 1.2139 THz, (b) 1.3118 THz, and (c) 1.3789 THz.

Authorized licensed use limited to: London Metropolitan University. Downloaded on March 13,2025 at 11:16:28 UTC from IEEE Xplore. Restrictions apply.
© 2025 IEEE. All rights reserved, including rights for text and data mining and training of artificial intelligence and similar technologies. Personal use is permitted,
but republication/redistribution requires IEEE permission. See https://www.ieee.org/publications/rights/index.html for more information.

This article has been accepted for publication in IEEE Sensors Journal. This is the author's version which has not been fully edited and
content may change prior to final publication. Citation information: DOI 10.1109/JSEN.2025.3545789

Figure 21 illustrates the distribution of the imaginary surface current within the proposed metamaterial structure at three distinct resonance frequencies. In Fig. 21(a), at 1.2139 THz, areas of high current intensity are represented in red, while regions with low intensity appear in blue. This visualization highlights how the surface current interacts with the metamaterial at this frequency, offering insights into its behavior and contribution to the resonance characteristics of the structure. Moving to Fig. 21(b), at 1.3118 THz, the distribution of surface current evolves, showing how the current intensity varies across the material at this higher frequency, which helps in understanding how the resonance properties of the material shift with frequency. Lastly, Figure 21(c), at 1.3789 THz, demonstrates how the surface current continues to change at an even higher frequency, further illustrating how the metamaterial's response to terahertz radiation varies as the frequency increases.

In Fig. 22(a), at 0.8619 THz, the real surface current is visualized with high current intensity regions shown in red and low intensity regions in blue. This distribution helps to understand how the real surface current interacts with the metamaterial at this frequency, contributing to the resonance behavior of the structure. In Fig. 22(b), at 0.9697 THz, the surface current distribution shifts, showing how the current intensity varies across the metamaterial at this slightly higher frequency. This provides insight into how the metamaterial's resonance characteristics change as the frequency increases. In Fig. 22(c), at 1.0544 THz, the surface current distribution continues to evolve, further illustrating how the material's response to terahertz radiation changes at this higher frequency.

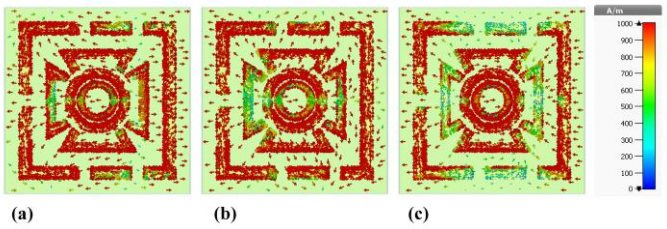

Figure 22: Real surface current distribution across the suggested metamaterial design at: (a) 0.8619 THz, (b) 0.9697 THz, and (c) 1.0544 THz.

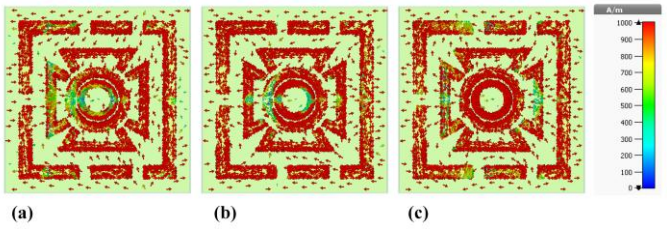

Figure 23: Visualization of the real surface current distribution in the recommended design, shown for frequencies: (a) 1.2139 THz, (b) 1.3118 THz, and (c) 1.3789 THz.

Figure 23 shows the real surface current distribution within the metamaterial structure at different resonance frequencies, highlighting variations in current intensity across the surface. Areas of high current intensity are shown in red, while low-intensity regions are depicted in blue, providing critical insights into the resonance behavior and energy transfer characteristics of the metamaterial. In Fig. 23(a), at 1.2139 THz, the surface current distribution reveals how the real surface current interacts with the metamaterial at this frequency, offering a deeper understanding of its resonance dynamics. As the frequency increases, Fig. 23(b), at 1.3118 THz, shows a shift in the current distribution, demonstrating how current intensity varies across the structure. This shift highlights the evolution of the metamaterial's resonance properties, reflecting changes in its electromagnetic response. At an even higher frequency, Fig. 23(c), at 1.3789 THz, further illustrates the continuous evolution of the surface current distribution, showing how the metamaterial interacts with terahertz radiation as the frequency increases.

By analyzing these distributions, we gain deeper insights into how the surface currents influence the metamaterial's electromagnetic properties, which directly impacts the sensor's performance. Precise control and optimization of surface currents are crucial in applications like terahertz-based biosensing, as they help improve the sensitivity, resolution, and overall performance of the sensor, particularly for detecting biological markers like cancer cells.

VI. Diagnosis of Breast Cancer

In this section, we discuss the application of the proposed metamaterial biosensor for the early detection and diagnosis of breast cancer. The ability to detect breast cancer at its earliest stages is crucial for effective treatment and improving survival rates. Traditional diagnostic methods, such as mammography, ultrasound, and biopsy, are widely used; however, they often come with limitations such as invasiveness, discomfort, and the potential for false positives or negatives. The integration of terahertz-based biosensing, particularly using metamaterials, offers a promising alternative for more accurate, non-invasive, and early detection of breast cancer.

The proposed metamaterial biosensor operates in the terahertz frequency range, which is highly sensitive to the molecular and biochemical properties of biological tissues. Cancerous tissues, such as MCF-7 breast cancer cells, exhibit distinct electromagnetic signatures due to alterations in cell structure, composition, and water content. These changes affect their dielectric properties, including the refractive index, which can serve as a critical marker for cancer detection. For instance, healthy breast tissue typically has a refractive index of 1.387, while MCF-7 breast cancer cells exhibit a slightly elevated refractive index of 1.401, reflecting these structural and biochemical differences [38, 66-70].

The biosensor leverages its unique multi-band resonant features to precisely analyze these variations, enabling the identification of cancerous cells with high sensitivity and selectivity. By analyzing the interactions of THz waves with tissue, the sensor can detect subtle changes in electromagnetic properties, facilitating early-stage diagnosis. This diagnostic capability is particularly valuable as it provides a label-free, non-invasive method to distinguish between normal and cancerous tissues based on their refractive index. The findings align with prior studies emphasizing the significance of refractive index differences in distinguishing healthy and malignant cells [22, 23, 25-30, 33, 35-45, 47-49].

Authorized licensed use limited to: London Metropolitan University. Downloaded on March 13,2025 at 11:16:28 UTC from IEEE Xplore. Restrictions apply.
© 2025 IEEE. All rights reserved, including rights for text and data mining and training of artificial intelligence and similar technologies. Personal use is permitted,
but republication/redistribution requires IEEE permission. See https://www.ieee.org/publications/rights/index.html for more information.

This article has been accepted for publication in IEEE Sensors Journal. This is the author's version which has not been fully edited and
content may change prior to final publication. Citation information: DOI 10.1109/JSEN.2025.3545789

This section explores how the metamaterial design, with its ability to operate within the critical 0.5 THz to 1.6 THz frequency range, enables the detection of breast cancer at a molecular level. The sharp resonance peaks of the sensor, as observed in various simulations, provide a clear and reproducible signature for cancerous tissue, making it a powerful tool for early diagnosis. Additionally, the sensor's non-invasive nature and potential for real-time analysis offer significant advantages over conventional diagnostic methods, making it a potential breakthrough in breast cancer detection.

Figure 24 illustrates the proposed biosensor setup, which is designed to evaluate the absorption coefficient in both healthy breast cells and MCF-7 breast cancer cells. The diagram shows a metamaterial-based sensor (MTMs sensor) interacting with the cancerous MCF-7 cells placed on a coverslip. The sensor is configured to measure the absorption characteristics of the cells, which is crucial for distinguishing cancerous cells from healthy ones.

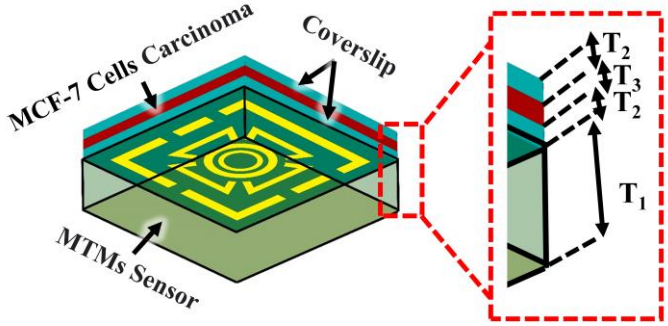

Figure 24: The proposed biosensor evaluates the absorption coefficient in both healthy breast cells and MCF-7 breast cancer cells.

The inset in the image highlights the interaction between the sensor and the cells, showing the multiple layers involved in the measurement. The labels T_1, T_2, and T_3 are the thickness of the layers in the sensor setup, which are important for determining the absorption of terahertz radiation at various frequencies. This setup enables the precise evaluation of how the cancerous tissue absorbs terahertz waves, offering a promising approach for early cancer detection. By analyzing these absorption properties, the biosensor can detect subtle differences between healthy and cancerous cells, providing valuable diagnostic information for breast cancer.

Figure 25 shows the absorption coefficient detection capabilities of the proposed biosensor across the frequency spectrum from 0.5 to 1.6 THz. In Fig. 25(a), the absorption coefficient for healthy breast tissue is shown, with the absorption peaks represented in blue. These peaks correspond to the interaction of terahertz waves with normal breast tissue, where the absorption characteristics are relatively stable, but exhibit variations at specific frequencies. In Fig. 25(b), the absorption coefficient for breast cancer tissue is shown in red. Compared to the healthy tissue, the cancerous tissue shows distinct and more pronounced absorption peaks. These differences in the absorption profiles between normal and cancerous tissue allow the biosensor to effectively differentiate between the two types, making it a promising tool for early detection of breast cancer.

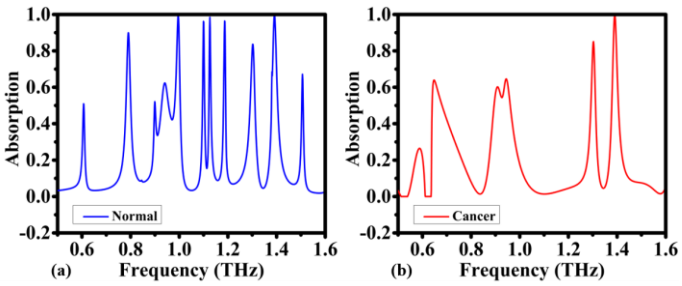

Figure 25: Demonstrates the absorption coefficient detection capabilities of the proposed biosensor across the frequency spectrum ranging from 0.5 to 1.6 THz, specifically illustrating: (a) healthy breast tissue, and (b) breast cancer tissue.

By analyzing these absorption spectra, the biosensor can identify subtle differences between healthy and cancerous breast tissue, providing critical diagnostic information for breast cancer detection. The frequency range of 0.5 to 1.6 THz is particularly useful in this context, as it captures the specific electromagnetic signatures that differentiate cancerous cells from normal ones.

Figure 26 illustrates the detection of MCF-7 breast cancer cells using the microwave imaging (MWI) technique. In this schematic, the MCF-7 cancer cells are placed on top of the metamaterial sensor, which is integrated with a coverslip. The sensor is designed to detect the electromagnetic characteristics of the MCF-7 cells, which differ from healthy cells, enabling the identification of cancerous tissue. The microwave imaging technique utilizes these differences in electromagnetic properties, offering a non-invasive method for detecting and diagnosing breast cancer. This setup is a promising approach for improving early cancer detection, as the microwave imaging technique can provide high-resolution, real-time analysis of cell interactions with terahertz waves.

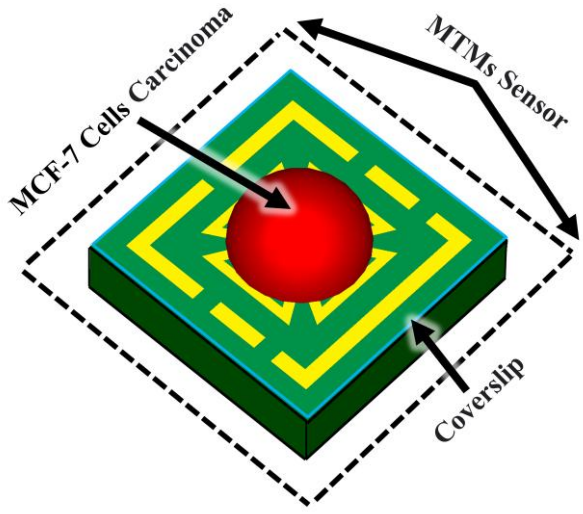

Figure 26: Detection of MCF-7 breast cancer cells using the microwave imaging (MWI) technique.

Figure 27 depicts the results of the electric field (E-field) microwave imaging method used for tissue differentiation between healthy and cancerous breast tissue. In Fig. 27(a), the image represents healthy breast tissue, with the electric field intensity shown in a color gradient ranging from green (low

Authorized licensed use limited to: London Metropolitan University. Downloaded on March 13,2025 at 11:16:28 UTC from IEEE Xplore. Restrictions apply.
© 2025 IEEE. All rights reserved, including rights for text and data mining and training of artificial intelligence and similar technologies. Personal use is permitted,
but republication/redistribution requires IEEE permission. See https://www.ieee.org/publications/rights/index.html for more information.

This article has been accepted for publication in IEEE Sensors Journal. This is the author's version which has not been fully edited and
content may change prior to final publication. Citation information: DOI 10.1109/JSEN.2025.3545789

intensity) to red (high intensity). The distribution indicates a more uniform and less intense interaction with the terahertz waves in healthy tissue. In Fig. 27(b), the image shows breast cancer tissue, where the electric field intensity is higher and more concentrated in the central area, highlighted in red. This contrast between the two tissue types is essential for identifying cancerous tissues, as the electromagnetic properties of cancerous cells differ significantly from healthy cells. The microwave imaging technique can help detect these differences with high precision, providing a non-invasive and effective approach for early breast cancer diagnosis.

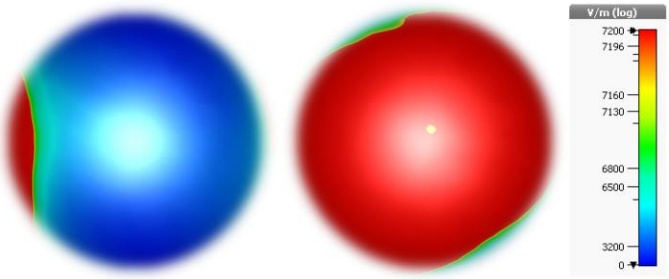

Figure 27: Depicts the outcomes of the electric field (E-field) microwave imaging method for tissue differentiation, showing (a) healthy breast tissue and (b) breast cancer tissue.

Figure 28 shows the results from the H-field microwave imaging approach, comparing healthy and breast cancer tissues. In Fig. 28(a), the image shows the magnetic field distribution for healthy breast tissue. The color gradient ranges from blue (low intensity) to green (higher intensity), with the field distribution being relatively uniform and diffuse, indicating a more standard interaction of the tissue with the terahertz waves. In Fig. 28(b), the image shows the magnetic field distribution for breast cancer tissue. In this case, the magnetic field intensity is more concentrated and shows a distinct pattern, with areas in red indicating regions of high intensity. The differences in the H-field between healthy and cancerous tissues provide critical information for differentiating the two types of tissue, as cancerous cells have distinct electromagnetic characteristics that alter the way they interact with microwave or terahertz radiation. This method can be an essential tool in non-invasive, early-stage breast cancer detection.

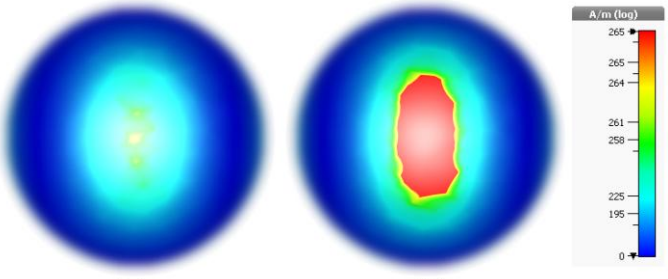

Figure 28: Shows the results derived from the magnetic field (H-field) microwave imaging approach, comparing: (a) healthy breast tissue with (b) breast cancer tissue.

VII. Comparison with State-of-the-Art Sensitivities

Table 2 presents a comparative analysis of various biosensors, demonstrating the exceptional performance of the proposed precision multi-band terahertz metamaterial biosensor. Notably, our biosensor achieves an unprecedented sensitivity of 138,700 THz/RIU, significantly surpassing the sensitivity values of previously reported biosensors, which range from 0.0242 THz/RIU [76] to a maximum of 174.87 THz/RIU [58]. Sensitivity is a crucial parameter in biosensing, as it determines the ability to detect minute changes in the refractive index of biological tissues, a key aspect of early-stage cancer diagnostics. The remarkable sensitivity of our biosensor highlights a substantial improvement over existing technologies, making it highly effective for detecting MCF-7 breast cancer cells.

TABLE 2
Bio-Sensing Performance Comparisons of Various Sensors and Applications Based on Metamaterial.

Ref.	S (THz/RIU)	FOM (RIU−1)	Q	Year Published	Bio-application
[25]	1.21	2.75	2.43	2022	Cancer Diagnosi, Biosensor
[26]	1.65	-	10.64	2021	Cancer detection
[27]	0.207	3.86	13	2022	Cancer detection
[28]	1.342, 2.78, 3.337	63.11, 84.134, 116.85	23.3, 24.1, 33.97	2024	Skin Cancer Diagnostics
[31]	2.2	-	927.5	2023	Dengue, Malaria, and Glucose Detection
[36]	0.074	-	-	2021	Cervical cancer
[37]	1.447	36.175	92.75	2022	Cancer Cell Detection
[38]	0.0515, 0.076	0.86, 1.15	12.8, 13.5	2023	Non-Melanoma Skin Cancer Diagnostics
[49]	0.042, 0.0704	1.9589, 1.529	20.382, 16.286	2024	Cervical Cancer Diagnosis
[58]	174.87	-	10.52, 11.94, 10.64, 12.09	2024	Breast cancer Detection
[74]	0.02432	0.1216	5.58	2014	detection of Penicillia
[75]	0. 203	1.81, 1.57	8.21, 6.05	2022	Sensor
[76]	0.0242, 0.02438	-	-	2017	detection of Virus
[77]	0. 960	-	-	2020	Biosensor, Collagen
[78]	0.285	1.88	6.6	2020	sensor
[79]	0. 2833	-	-	2021	Polystyrene particle
[80]	1.06	0.166	-	2022	detection of avian influenza virus
[81]	0.068	-	-	2022	Hepatocellular carcinoma
[82]	0.278	-	11	2023	Bovin serum albumin protein
[83]	0.495	-	82	2023	Cancer detection
This work	138700	14010101	122727	-	Breast cancer

In addition to sensitivity, the Figure of Merit (FOM) of the proposed biosensor is extraordinarily high, reaching 14,010,101 RIU^{-1}, which far exceeds the values reported in previous studies. As indicated in Table 2, biosensors in the literature exhibit FOM values ranging from 0.1216 RIU^{-1} [74] to 116.85 RIU^{-1} [28]. The exceptionally high FOM of our

Authorized licensed use limited to: London Metropolitan University. Downloaded on March 13,2025 at 11:16:28 UTC from IEEE Xplore. Restrictions apply.
© 2025 IEEE. All rights reserved, including rights for text and data mining and training of artificial intelligence and similar technologies. Personal use is permitted,
but republication/redistribution requires IEEE permission. See https://www.ieee.org/publications/rights/index.html for more information.

This article has been accepted for publication in IEEE Sensors Journal. This is the author's version which has not been fully edited and
content may change prior to final publication. Citation information: DOI 10.1109/JSEN.2025.3545789

biosensor ensures sharp resonance peaks, enhancing spectral selectivity and minimizing interference from background noise. This characteristic is critical for precise differentiation between healthy and cancerous tissues, even in complex biological environments.

Another key performance metric is the quality factor (Q-factor), which reflects the biosensor's ability to maintain narrow resonance peaks, improving spectral resolution and detection accuracy. Our biosensor achieves a Q-factor of 122,727, which significantly surpasses the values reported for comparable technologies, as seen in Table 2. For instance, previously reported biosensors exhibit Q-factors ranging from as low as 2.43 [25] to a maximum of 927.5 [31], highlighting the superior resonance characteristics of our design. A high Q-factor is essential for detecting subtle electromagnetic signatures associated with MCF-7 breast cancer cells, enabling high-precision, multi-band detection.

Furthermore, the biosensor exhibits an absorptivity exceeding 99% across the 0.5–1.6 THz operating range, ensuring maximum interaction with biomolecules and enhancing detection efficiency. When benchmarked against state-of-the-art biosensors, our design not only outperforms in terms of sensitivity, FOM, and Q-factor but also integrates these capabilities into a compact and multi-band architecture, making it highly suitable for real-time, non-invasive cancer diagnostics.

Collectively, these advancements position our multi-band terahertz metamaterial biosensor as a groundbreaking tool for early-stage breast cancer detection, offering a significant improvement over existing and emerging biosensing technologies.

VIII. Benchmarking

The proposed multi-band terahertz metamaterial biosensor demonstrates exceptional performance when benchmarked against existing biosensors, as detailed in Tables 2 and 3. Operating within the 0.5–1.6 THz frequency range, the sensor is specifically optimized for biosensing applications by leveraging the unique spectral window associated with the vibrational and intermolecular interaction modes of biomolecules, including MCF-7 breast cancer cells. This targeted frequency range enables precise detection of refractive index changes, a critical parameter for identifying cellular abnormalities indicative of malignancy.

A standout feature of the proposed biosensor is its ultra-high sensitivity of 138,700 THz/RIU, which significantly surpasses previously reported values, as shown in Table 2, where sensitivity ranges between 0.05 and 1.06 THz/RIU [80]. The exceptional sensitivity ensures the detection of even minute refractive index variations caused by the presence of target analytes, a crucial factor for early-stage cancer diagnosis. Additionally, the biosensor achieves an outstanding Figure of Merit (FOM) of 14,010,101 RIU^{-1}, far exceeding reported values that range between 0.1216 RIU^{-1} [74] and 116.85 RIU^{-1} [28]. This high FOM ensures sharp resonance peaks with minimal noise, enhancing spectral selectivity and improving diagnostic accuracy. Moreover, the quality factor (Q-factor) of 122,727 further reinforces the biosensor's capability to produce narrow resonance peaks, enabling high-resolution spectral detection.

The multi-band resonance design, characterized by six distinct resonance peaks, provides a substantial advantage in spectral targeting. These sharp and well-defined peaks allow for the selective interrogation of specific biological markers, improving the differentiation of cancerous cells compared to biosensors with broader or single-band responses. Unlike broadband sensors such as those in Refs. [71] and [72], which cover a wider frequency range but lack spectral precision, the proposed biosensor ensures high specificity in spectral discrimination, making it a more effective tool for biomedical diagnostics.

Another key feature of the biosensor is its exceptional absorptivity, exceeding 99% across its operating frequencies. This high absorption efficiency ensures maximum interaction between terahertz radiation and the target analyte, further enhancing sensitivity. In contrast, previously reported biosensors demonstrate absorptivity values of 0.97–0.98 [25, 72], underscoring the superior detection efficiency of the proposed design. As detailed in Table 3, the proposed biosensor, utilizing an Al/PET/Al configuration, achieves absorptivity levels ranging from 0.986 to 0.9995, which is among the highest recorded values for metamaterial-based biosensors.

The metamaterial-based architecture of the sensor offers distinct advantages by leveraging engineered electromagnetic properties that are not achievable in natural materials. These properties enable strong electromagnetic field confinement and enhancement at the micronscale, significantly improving light-matter interactions. The biosensor's compact footprint (198 × 198 μm^2) ensures portability and facilitates seamless integration with microwave imaging (MWI) systems for real-time, non-invasive cancer diagnostics. This capability sets it apart from other biosensing devices, including those developed for virus detection or broadband sensing applications [71, 73].

In conclusion, the benchmarking results clearly establish that the proposed multi-band terahertz metamaterial biosensor surpasses existing biosensors in terms of sensitivity, FOM, absorptivity, and spectral specificity, making it a highly specialized tool for early-stage breast cancer detection. Its innovative metamaterial design, coupled with integration into advanced diagnostic techniques, provides significant enhancements in diagnostic accuracy, efficiency, and portability, paving the way for next-generation clinical applications.

IX. Future Perspective

The precision multi-band terahertz metamaterial biosensor introduces a transformative approach to cancer diagnostics, specifically for detecting MCF-7 breast cancer cells. Future advancements could focus on integrating this sensor with point-of-care devices, enabling real-time, portable, and cost-effective cancer screening. Expanding its operational spectrum to address other cancer types or diseases will further broaden its clinical applicability.

Incorporating vivo testing and optimizing sensor miniaturization for clinical trials can validate its effectiveness

Authorized licensed use limited to: London Metropolitan University. Downloaded on March 13,2025 at 11:16:28 UTC from IEEE Xplore. Restrictions apply.
© 2025 IEEE. All rights reserved, including rights for text and data mining and training of artificial intelligence and similar technologies. Personal use is permitted,
but republication/redistribution requires IEEE permission. See https://www.ieee.org/publications/rights/index.html for more information.

This article has been accepted for publication in IEEE Sensors Journal. This is the author's version which has not been fully edited and content may change prior to final publication. Citation information: DOI 10.1109/JSEN.2025.3545789

in practical settings. Additionally, leveraging artificial intelligence for data interpretation could enhance diagnostic accuracy and streamline clinical workflows. This biosensor's potential to redefine non-invasive diagnostics underscores its pivotal role in advancing precision medicine.

TABLE 3
A COMPARISON BETWEEN THE PROPOSED METAMATERIAL BASED BIOSENSOR AND OTHER BIOSENSORS.

Ref.	Application	Frequency operating THz	Material substrate	Techniques used	Absorptivity
[25]	Breast cancer detection	0.5-2.5	SiO_2	SiO_2/Graphene	-
[71]	Multi-Frequency Broadband and Ultra-Broadband	7-9.5	SiO_2	Au/ SiO_2/ Graphene	0.98
[72]	biosensor for detecting coronaviruses	1.5-1.7	silicon dioxide	Gold/silicon dioxide/ Gold	0.972, 0.991
[73]	Refractive index sensor	2−6	SiO_2	graphene/Au/SiO_2/Au	0.99
[84]	Colon Cancer Detection	0-0.37	Glass	Glass/InSb/MgF2/InSb	0.998
[85]	Narrowband perfect absorber	1−3	photonic crystal plate	bulk Dirac semimetal/photonic crystal/Au	0.97, 0.98, 0.99
[86]	Sensor	1−3	dielectric layer	Au/dielectric layer/Au	0.99, 0.99
[87]	Multifunctional Tunable Terahertz	0-3	PET	PET/FSS/UV glue/ Graphene	0.99, 0.80, 0.95
[88]	polarization-sensitive	0.7-5	Teflon	Ion gel/Graphene/Teflon/Gold	>0.96
[89]	Ultra-Broadband Absorber	0.5−4.5	Topas spacer	graphene/Topas/Au	0.99, 0.98, 0.99
[90]	Sensor	1−2.2	dielectric Teflon	Au/dielectric Teflon/Au	0.99
This work	MCF-7 Breast cancer, Microwave Imaging and Biosensor	0.5−1.6	PET	Al/ PET /Al	0.99, 0.9995, 0.996, 0.998, 0.986, 0.995

X. CONCLUSIONS

The precision multi-band terahertz metamaterial biosensor represents a breakthrough in biosensing, particularly for the early detection of MCF-7 breast cancer cells. By harnessing the unique properties of terahertz radiation and metamaterials, this biosensor achieves exceptional sensitivity, spectral selectivity, and accuracy, setting it apart from conventional biosensing technologies. Its multi-band resonance design, featuring six sharp resonance peaks within the 0.5–1.6 THz range, allows for precise detection of cancerous tissues. Unlike other sensors with broader frequency ranges or less focused designs, this targeted approach significantly enhances detection accuracy and specificity.

A key advantage of this biosensor is its ultra-high sensitivity of 138,700 THz/RIU, which enables the detection of even minute changes in the refractive index, outperforming traditional biosensors in detection capability. Additionally, its high Figure of Merit (FOM) of 14,010,101 RIU^{-1} and quality factor (Q) of 122,727 further enhance spectral specificity, making it highly effective for identifying biological analytes with precision. The biosensor also demonstrates near-perfect absorption (>99%) at its resonance frequencies, maximizing biomolecular interaction and ensuring highly accurate detection. The integration of strong electromagnetic field confinement, supported by metamaterials, enhances light-matter interactions at the microscale, a critical factor for high-performance biosensing.

Furthermore, the biosensor incorporates microfluidic coupling, which significantly improves sensitivity by detecting even the smallest changes in the dielectric properties of biological tissues. This capability enhances real-time detection and makes the sensor suitable for non-invasive diagnostics. Its compact footprint (198 × 198 μm^2) ensures portability and facilitates seamless integration into clinical applications, offering a fast, reliable, and minimally invasive alternative to conventional cancer detection methods.

This work underscores the transformative potential of terahertz metamaterial biosensors in revolutionizing cancer diagnostics. The proposed biosensor provides a faster, more reliable, and highly sensitive approach for detecting MCF-7 breast cancer cells, paving the way for early intervention and improved treatment outcomes. As research continues to refine and optimize these technologies, the precision multi-band terahertz metamaterial biosensor stands as a promising candidate for next-generation oncology diagnostics, driving advancements in non-invasive, real-time cancer detection.

REFERENCES

[1] W. Cao, H.-D. Chen, Y.-W. Yu, N. Li, and W.-Q. Chen, "Changing profiles of cancer burden worldwide and in China: a secondary analysis of the global cancer statistics

Authorized licensed use limited to: London Metropolitan University. Downloaded on March 13,2025 at 11:16:28 UTC from IEEE Xplore. Restrictions apply.
© 2025 IEEE. All rights reserved, including rights for text and data mining and training of artificial intelligence and similar technologies. Personal use is permitted, but republication/redistribution requires IEEE permission. See https://www.ieee.org/publications/rights/index.html for more information.

This article has been accepted for publication in IEEE Sensors Journal. This is the author's version which has not been fully edited and
content may change prior to final publication. Citation information: DOI 10.1109/JSEN.2025.3545789

2020," *Chinese medical journal,* vol. 134, no. 07, pp. 783-791, 2021.

[2] V. Kumar, D. Kukkar, B. Hashemi, K. H. Kim, and A. Deep, "Advanced Functional Structure-Based Sensing and Imaging Strategies for Cancer Detection: Possibilities, Opportunities, Challenges, and Prospects," *Advanced Functional Materials,* vol. 29, no. 16, p. 1807859, 2019.

[3] H. Sung *et al.*, "Global cancer statistics 2020: GLOBOCAN estimates of incidence and mortality worldwide for 36 cancers in 185 countries," *CA: a cancer journal for clinicians,* vol. 71, no. 3, pp. 209-249, 2021.

[4] J. Ferlay *et al.*, "Cancer statistics for the year 2020: An overview," *International journal of cancer,* vol. 149, no. 4, pp. 778-789, 2021.

[5] M. Pourmadadi *et al.*, "Construction of aptamer-based nanobiosensor for breast cancer biomarkers detection utilizing g-C3N4/magnetic nano-structure," *Biosensors,* vol. 12, no. 11, p. 921, 2022.

[6] J. Quan, Y. Wang, J. Zhang, K. Huang, X. Wang, and H. Jiang, "Aptamer embedded arch-cruciform DNA assemblies on 2-D VS2 scaffolds for sensitive detection of breast cancer cells," *Biosensors,* vol. 11, no. 10, p. 378, 2021.

[7] N. Harbeck *et al.*, "Breast cancer Nat Rev Dis Primers 5: 66," ed, 2019.

[8] R. Siegal, K. Miller, and A. Jemal, "Cancer statistics, 2012," *Ca Cancer J Clin,* vol. 64, no. 1, pp. 9-29, 2014.

[9] L. A. Torre, F. Islami, R. L. Siegel, E. M. Ward, and A. Jemal, "Global cancer in women: burden and trends," *Cancer epidemiology, biomarkers & prevention,* vol. 26, no. 4, pp. 444-457, 2017.

[10] N. Pashayan and P. D. Pharoah, "The challenge of early detection in cancer," *Science,* vol. 368, no. 6491, pp. 589-590, 2020.

[11] Y. Van Der Pol and F. Mouliere, "Toward the early detection of cancer by decoding the epigenetic and environmental fingerprints of cell-free DNA," *Cancer cell,* vol. 36, no. 4, pp. 350-368, 2019.

[12] N. Grivas *et al.*, "Prostate cancer detection percentages of repeat biopsy in patients with positive multiparametric magnetic resonance imaging (prostate imaging reporting and data system/likert 3–5) and negative initial biopsy. A mini systematic review," *European Urology,* vol. 82, no. 5, pp. 452-457, 2022.

[13] B. P. Joshi *et al.*, "Detection of sessile serrated adenomas in the proximal colon using wide-field fluorescence endoscopy," *Gastroenterology,* vol. 152, no. 5, pp. 1002-1013. e9, 2017.

[14] M. Ignatiadis, G. W. Sledge, and S. S. Jeffrey, "Liquid biopsy enters the clinic—implementation issues and future challenges," *Nature reviews Clinical oncology,* vol. 18, no. 5, pp. 297-312, 2021.

[15] M. A. Mir and M. S. Tirumkudulu, "A low-cost flow cell for flow cytometry," *Biosensors and Bioelectronics,* vol. 211, p. 114334, 2022.

[16] H. K. Gaikwad, D. Tsvirkun, Y. Ben-Nun, E. Merquiol, R. Popovtzer, and G. Blum, "Molecular imaging of cancer using X-ray computed tomography with protease targeted iodinated activity-based probes," *Nano letters,* vol. 18, no. 3, pp. 1582-1591, 2018.

[17] H. Ji, T. W. Kim, W. J. Lee, S. D. Jeong, Y. B. Cho, and H. H. Kim, "Two circPPFIA1s negatively regulate liver metastasis of colon cancer via miR-155-5p/CDX1 and HuR/RAB36," *Molecular Cancer,* vol. 21, no. 1, p. 197, 2022.

[18] M. Danaie and B. Kiani, "Design of a label-free photonic crystal refractive index sensor for biomedical applications," *Photonics and nanostructures-fundamentals and applications,* vol. 31, pp. 89-98, 2018.

[19] S. P. Mickan *et al.*, "Label-free bioaffinity detection using terahertz technology," *Physics in Medicine & Biology,* vol. 47, no. 21, p. 3789, 2002.

[20] S. Smye, J. Chamberlain, A. Fitzgerald, and E. Berry, "The interaction between terahertz radiation and biological tissue," *Physics in Medicine & Biology,* vol. 46, no. 9, p. R101, 2001.

[21] X. Zhan, Y. Liu, Z. Chen, J. Luo, S. Yang, and X. Yang, "Revolutionary approaches for cancer diagnosis by terahertz-based spectroscopy and imaging," *Talanta,* vol. 259, p. 124483, 2023.

[22] M. Rezeg, A. Hlali, and H. Zairi, "THz Biomedical Sensing for Early Cancer Detection: Metamaterial Graphene Biosensors with Rotated Split-Ring Resonators," *IEEE Photonics Journal,* 2024.

[23] L. Yu *et al.*, "The medical application of terahertz technology in non-invasive detection of cells and tissues: opportunities and challenges," *RSC advances,* vol. 9, no. 17, pp. 9354-9363, 2019.

[24] G. Valušis, A. Lisauskas, H. Yuan, W. Knap, and H. G. Roskos, "Roadmap of terahertz imaging 2021," *Sensors,* vol. 21, no. 12, p. 4092, 2021.

[25] C. Tan *et al.*, "Cancer Diagnosis Using Terahertz-Graphene-Metasurface-Based Biosensor with Dual-Resonance Response," *Nanomaterials,* vol. 12, no. 21, p. 3889, 2022.

[26] M. Y. Azab, M. F. O. Hameed, A. M. Nasr, and S. Obayya, "Highly sensitive metamaterial biosensor for cancer early detection," *IEEE Sensors Journal,* vol. 21, no. 6, pp. 7748-7755, 2021.

[27] S. K. Patel, J. Surve, and J. Parmar, "Detection of cancer with graphene metasurface-based highly efficient sensors," *Diamond and Related Materials,* vol. 129, p. 109367, 2022.

[28] M. N. Hamza *et al.*, "Designing a High-sensitivity Microscale Triple-band Biosensor based on Terahertz MTMs to provide a perfect absorber for Non-Melanoma Skin Cancer diagnostic," *IEEE Photonics Journal,* 2024.

[29] B. Amini and Z. Atlasbaf, "Design and analysis of high-sensitivity tunable graphene sensors for cancer detection," *Optical and Quantum Electronics,* vol. 55, no. 5, p. 446, 2023.

[30] M. N. Hamza and M. T. Islam, "Design of MTM-based Multi-band Micro-Biosensor in Terahertz region as perfect absorber for Early-Stage Leukemia Diagnosis with sensitivity 18626373 THz/RIU," *IEEE Sensors Journal,* 2024.

[31] P. Upender and A. Kumar, "THz dielectric metamaterial sensor with high Q for biosensing applications," *IEEE Sensors Journal,* vol. 23, no. 6, pp. 5737-5744, 2023.

[32] M. N. Hamza, S. Koziel, and A. Pietrenko-Dabrowska, "Design and experimental validation of a metamaterial-based sensor for microwave imaging in breast, lung, and brain cancer detection," *Scientific Reports,* vol. 14, no. 1, p. 16177, 2024.

[33] Z. Geng, X. Zhang, Z. Fan, X. Lv, and H. Chen, "A route to terahertz metamaterial biosensor integrated with microfluidics for liver cancer biomarker testing in early stage," *Scientific reports,* vol. 7, no. 1, p. 16378, 2017.

[34] S. Banerjee, U. Nath, P. Dutta, A. V. Jha, B. Appasani, and N. Bizon, "A theoretical terahertz metamaterial absorber structure with a high quality factor using two circular ring

Authorized licensed use limited to: London Metropolitan University. Downloaded on March 13,2025 at 11:16:28 UTC from IEEE Xplore. Restrictions apply.
© 2025 IEEE. All rights reserved, including rights for text and data mining and training of artificial intelligence and similar technologies. Personal use is permitted,
but republication/redistribution requires IEEE permission. See https://www.ieee.org/publications/rights/index.html for more information.

This article has been accepted for publication in IEEE Sensors Journal. This is the author's version which has not been fully edited and
content may change prior to final publication. Citation information: DOI 10.1109/JSEN.2025.3545789

resonators for biomedical sensing," *Inventions*, vol. 6, no. 4, p. 78, 2021.

[35] H. E. Nejad, A. Mir, and A. Farmani, "Supersensitive and tunable nano-biosensor for cancer detection," *IEEE Sensors Journal*, vol. 19, no. 13, pp. 4874-4881, 2019.

[36] D. Li *et al.*, "Identification of early-stage cervical cancer tissue using metamaterial terahertz biosensor with two resonant absorption frequencies," *IEEE Journal of Selected Topics in Quantum Electronics*, vol. 27, no. 4, pp. 1-7, 2021.

[37] S. Banerjee, P. Dutta, A. V. Jha, B. Appasani, and M. S. Khan, "A biomedical sensor for detection of cancer cells based on terahertz metamaterial absorber," *IEEE Sensors Letters*, vol. 6, no. 6, pp. 1-4, 2022.

[38] M. N. Hamza and M. T. Islam, "Designing an Extremely Tiny Dual-Band Biosensor Based on MTMs in the Terahertz Region as a Perfect Absorber for Non-Melanoma Skin Cancer Diagnostics," *IEEE Access*, vol. 11, pp. 136770-136781, 2023.

[39] A. Chaudhuri, B. Rai, and P. Pal, "Design of a dual-band metasurface cross-polarization converter for cancer detection in the terahertz band," *IEEE Sensors Journal*, vol. 24, no. 6, pp. 7292-7298, 2023.

[40] J. Chen, F. Hu, X. Ma, M. Yang, S. Lin, and A. Su, "Deep neural network assisted terahertz metasurface sensors for the detection of lung cancer biomarkers," *IEEE Sensors Journal*, 2024.

[41] M. N. Hamza, M. T. Islam, S. Lavadiya, S. Koziel, I. Ud Din, and B. Sanches, "Designing a High-sensitivity Dual-band Nano-Biosensor based on Petahertz MTMs to provide a perfect absorber for Early-Stage Non-Melanoma Skin Cancer diagnostic," *IEEE Sensors Journal*, 2024.

[42] A. Hlali, A. Oueslati, and H. Zairi, "Numerical simulation of tunable terahertz graphene-based sensor for breast tumor detection," *IEEE Sensors Journal*, vol. 21, no. 8, pp. 9844-9851, 2021.

[43] X. Hou *et al.*, "Cancer biomarkers ultrasensitive detection based on terahertz frequency-comb-like," *IEEE Sensors Journal*, vol. 23, no. 10, pp. 10413-10419, 2023.

[44] M. N. Hamza *et al.*, "Development of a Terahertz Metamaterial Micro-Biosensor for Ultrasensitive Multispectral Detection of Early-Stage Cervical Cancer," *IEEE Sensors Journal*, 2024.

[45] A. Veeraselvam, G. N. A. Mohammed, K. Savarimuthu, and P. D. Vijayaraman, "An ultra-thin multiband refractive index-based carcinoma sensor using THz radiation," *IEEE Sensors Journal*, vol. 22, no. 3, pp. 2045-2052, 2021.

[46] M. N. Hamza *et al.*, "Ultra-compact quintuple-band terahertz metamaterial biosensor for enhanced blood cancer diagnostics," *PLOS ONE*, vol. 20, no. 1, p. e0313874, 2025.

[47] D. Xie *et al.*, "Terahertz metamaterial biosensor with double resonant frequencies for specific detection of early-stage hepatocellular carcinoma," *IEEE Sensors Journal*, vol. 23, no. 2, pp. 1124-1131, 2022.

[48] F. Wahaia *et al.*, "Detection of colon cancer by terahertz techniques," *Journal of Molecular Structure*, vol. 1006, no. 1-3, pp. 77-82, 2011.

[49] M. N. Hamza *et al.*, "Terahertz dual-band metamaterial biosensor for cervical-cancer diagnostics," *IEEE Photonics Journal*, 2024.

[50] W. Zhang *et al.*, "Terahertz metamaterials for biosensing applications: A review," *Biosensors*, vol. 14, no. 1, p. 3, 2023.

[51] M. N. Hamza, M. T. Islam, and S. Koziel, "Advanced sensor for non-invasive breast cancer and brain cancer diagnosis using antenna array with metamaterial-based AMC," *Engineering Science and Technology, an International Journal*, vol. 56, p. 101779, 2024.

[52] W. Fang, X. Lv, Z. Ma, J. Liu, W. Pei, and Z. Geng, "A flexible terahertz metamaterial biosensor for cancer cell growth and migration detection," *Micromachines*, vol. 13, no. 4, p. 631, 2022.

[53] E. S. McDonald, A. S. Clark, J. Tchou, P. Zhang, and G. M. Freedman, "Clinical diagnosis and management of breast cancer," *Journal of Nuclear Medicine*, vol. 57, no. Supplement 1, pp. 9S-16S, 2016.

[54] N. F. Pondé, D. Zardavas, and M. Piccart, "Progress in adjuvant systemic therapy for breast cancer," *Nature reviews Clinical oncology*, vol. 16, no. 1, pp. 27-44, 2019.

[55] A. Mohammadpour-Haratbar, S. B. A. Boraei, Y. Zare, K. Y. Rhee, and S.-J. Park, "Graphene-based electrochemical biosensors for breast cancer detection," *Biosensors*, vol. 13, no. 1, p. 80, 2023.

[56] Y. Deng, Y. Zhang, M. Zhou, B. Wu, and J. Zhou, "Application of Biosensors in Detecting Breast Cancer Metastasis," *Sensors*, vol. 23, no. 21, p. 8813, 2023.

[57] Y. Yang, Y. Fu, H. Su, L. Mao, and M. Chen, "Sensitive detection of MCF-7 human breast cancer cells by using a novel DNA-labeled sandwich electrochemical biosensor," *Biosensors and Bioelectronics*, vol. 122, pp. 175-182, 2018.

[58] T. Kamani, S. K. Patel, O. Alsalman, and F. Alsaif, "Design and optimization of refractive index biosensor for MDA-MB-231 and MCF-7 breast cancer biomarker detection," *Physica Scripta*, vol. 99, no. 10, p. 105541, 2024.

[59] M. Rahmanipour *et al.*, "Precision in cancer diagnostics: ultra-sensitive detection of MCF-7 breast cancer cells by gold nanostructure-enhanced electrochemical biosensing," *Journal of Materials Chemistry B*, vol. 12, no. 22, pp. 5551-5560, 2024.

[60] G. Wang, F. Zhu, T. Lang, J. Liu, Z. Hong, and J. Qin, "All-metal terahertz metamaterial biosensor for protein detection," *Nanoscale research letters*, vol. 16, pp. 1-10, 2021.

[61] S. Shen *et al.*, "Recent advances in the development of materials for terahertz metamaterial sensing," *Advanced Optical Materials*, vol. 10, no. 1, p. 2101008, 2022.

[62] H. Bi, M. Yang, and R. You, "Advances in terahertz metasurface graphene for biosensing and application," *Discover Nano*, vol. 18, no. 1, p. 63, 2023.

[63] M. Zhang *et al.*, "Exploring the application of multi-resonant bands terahertz metamaterials in the field of carbohydrate films sensing," *Biosensors*, vol. 13, no. 6, p. 606, 2023.

[64] J. LIU, "Research on a terahertz metamaterial biosensor with integrated microfluidic," *Journal of Optoelectronics and Advanced Materials*, vol. 26, no. January-February 2024, pp. 9-17, 2024.

[65] R. Bhati and A. K. Malik, "Multiband terahertz metamaterial perfect absorber for microorganisms detection," *Scientific Reports*, vol. 13, no. 1, p. 19685, 2023.

[66] K. Ahmed, B. K. Paul, F. Ahmed, M. A. Jabin, and M. S. Uddin, "Numerical demonstration of triangular shaped photonic crystal fibre-based biosensor in the Terahertz range," *IET Optoelectronics*, vol. 15, no. 1, pp. 1-7, 2021.

[67] M. A. Jabin *et al.*, "Surface plasmon resonance based titanium coated biosensor for cancer cell detection," *IEEE Photonics Journal*, vol. 11, no. 4, pp. 1-10, 2019.

Authorized licensed use limited to: London Metropolitan University. Downloaded on March 13,2025 at 11:16:28 UTC from IEEE Xplore. Restrictions apply.
© 2025 IEEE. All rights reserved, including rights for text and data mining and training of artificial intelligence and similar technologies. Personal use is permitted,
but republication/redistribution requires IEEE permission. See https://www.ieee.org/publications/rights/index.html for more information.

This article has been accepted for publication in IEEE Sensors Journal. This is the author's version which has not been fully edited and
content may change prior to final publication. Citation information: DOI 10.1109/JSEN.2025.3545789

[68] P. Kumar, V. Kumar, and J. S. Roy, "Dodecagonal photonic crystal fibers with negative dispersion and low confinement loss," *Optik*, vol. 144, pp. 363-369, 2017.

[69] T. Parvin, K. Ahmed, A. M. Alatwi, and A. N. Z. Rashed, "Differential optical absorption spectroscopy-based refractive index sensor for cancer cell detection," *Optical Review*, vol. 28, pp. 134-143, 2021.

[70] P. Sharma, P. Sharan, and P. Deshmukh, "A photonic crystal sensor for analysis and detection of cancer cells," in *2015 International conference on pervasive computing (ICPC)*, 2015, pp. 1-5: IEEE.

[71] Z. Chen *et al.*, "Graphene Multi-Frequency Broadband and Ultra-Broadband Terahertz Absorber Based on Surface Plasmon Resonance," *Electronics*, vol. 12, no. 12, p. 2655, 2023.

[72] Z. El-Wasif, T. Ismail, and O. Hamdy, "Design and optimization of highly sensitive multi-band terahertz metamaterial biosensor for coronaviruses detection," *Optical and Quantum Electronics*, vol. 55, no. 7, p. 604, 2023.

[73] M.-R. Nickpay, M. Danaie, and A. Shahzadi, "Highly sensitive THz refractive index sensor based on folded split-ring metamaterial graphene resonators," *Plasmonics*, pp. 1-12, 2021.

[74] S. Park *et al.*, "Detection of microorganisms using terahertz metamaterials," *Scientific reports*, vol. 4, no. 1, p. 4988, 2014.

[75] H. Hu, B. Qi, Y. Zhao, X. Zhang, Y. Wang, and X. Huang, "A graphene-based THz metasurface sensor with air-spaced structure," *Frontiers in Physics*, vol. 10, p. 990126, 2022.

[76] S. Park, S. Cha, G. Shin, and Y. Ahn, "Sensing viruses using terahertz nano-gap metamaterials," *Biomedical optics express*, vol. 8, no. 8, pp. 3551-3558, 2017.

[77] S. Asgari, N. Granpayeh, and T. Fabritius, "Controllable terahertz cross-shaped three-dimensional graphene intrinsically chiral metastructure and its biosensing application," *Optics Communications*, vol. 474, p. 126080, 2020.

[78] T. Chen, D. Zhang, F. Huang, Z. Li, and F. Hu, "Design of a terahertz metamaterial sensor based on split ring resonator nested square ring resonator," *Materials Research Express*, vol. 7, no. 9, p. 095802, 2020.

[79] J. Yang and Y.-S. Lin, "Design of tunable terahertz metamaterial sensor with single-and dual-resonance characteristic," *Nanomaterials*, vol. 11, no. 9, p. 2212, 2021.

[80] E. Hoseini, A. Mir, and A. Farmani, "Modeling and proposal of a black phosphorus-based nanostructure for detection of avian influenza virus in infrared region," *Optical and Quantum Electronics*, vol. 54, no. 10, p. 609, 2022.

[81] R. Bhati and A. K. Malik, "Ultra-efficient terahertz metamaterial sensor," *Results in Optics*, vol. 8, p. 100236, 2022.

[82] Y. Shen *et al.*, "Low-Concentration Biological Sample Detection Using an Asymmetric Split Resonator Terahertz Metamaterial," in *Photonics*, 2023, vol. 10, no. 2, p. 111: MDPI.

[83] Z. Mezache, Z. Hafdi, and J. Tao, "Design of a novel graphene buzzle metamaterial refractometer for sensing of cancerous cells in the terahertz regime," *Optik*, vol. 287, p. 171170, 2023.

[84] Z. Vafapour, W. Troy, and A. Rashidi, "Colon cancer detection by designing and analytical evaluation of a water-based THz metamaterial perfect absorber," *IEEE Sensors Journal*, vol. 21, no. 17, pp. 19307-19313, 2021.

[85] Y. Wang *et al.*, "Terahertz tunable three band narrowband perfect absorber based on Dirac semimetal," *Physica E: Low-dimensional Systems and Nanostructures*, vol. 131, p. 114750, 2021.

[86] B.-X. Wang, Y. He, P. Lou, and W. Xing, "Design of a dual-band terahertz metamaterial absorber using two identical square patches for sensing application," *Nanoscale Advances*, vol. 2, no. 2, pp. 763-769, 2020.

[87] S. Zhuang *et al.*, "Graphene-Based Absorption–Transmission Multi-Functional Tunable THz Metamaterials," *Micromachines*, vol. 13, no. 8, p. 1239, 2022.

[88] S. Asgari and T. Fabritius, "Numerical Simulation and Equivalent Circuit Model of Multi-Band Terahertz Absorber Composed of Double-Sided Graphene Comb Resonator Array," *IEEE Access*, 2023.

[89] L. Liu, W. Liu, and Z. Song, "Ultra-broadband terahertz absorber based on a multilayer graphene metamaterial," *Journal of Applied Physics*, vol. 128, no. 9, 2020.

[90] A. S. Saadeldin, M. F. O. Hameed, E. M. Elkaramany, and S. S. Obayya, "Highly sensitive terahertz metamaterial sensor," *IEEE Sensors Journal*, vol. 19, no. 18, pp. 7993-7999, 2019.

MUSA N. HAMZA received the B.Sc. degree from the Department of Physics, Faculty of Science and Health, Koya University, Koysinjaq, Erbil, Iraqi Kurdistan, Iraq, in 2015, and the M.Sc. degree from the Department of Medical Physics, College of Medical and Applied Sciences, Charmo University, Chamchamal, Sulaymaniyah, in 2023. His research interests include medical physics, the diagnosis of different types of cancer at an early stage, antenna arrays, metamaterials, sensors, and biosensors.

Mohammad Alibakhshikenari (Member, IEEE) was born in Mazandaran, Iran, in February 1988. He received the Ph.D. degree with the European label and Excellent Cum Laude in electronics engineering from the University of Rome ‘‘Tor Vergata’’ (UNITOV), Italy, in February 2020. From May to December 2018, he was a Ph.D. Visiting Researcher with the Chalmers University of Technology, Gothenburg, Sweden. His training during this visit included a research stage at Swedish Company ‘‘Gap Waves AB.’’ During the Ph.D. degree (November 2016 to February 2020), he has attended 13 European doctoral schools organized by various European universities and organizations, and he successfully achieved all the credits leading him to obtain the Ph.D. degree with European label. In November 2019, he was winner of a postdoctoral research fund for two years awarded by UNITOV. From July 2021 to August 2024, he was with the Department of Signal Theory and Communications, Universidad Carlos III de Madrid (UC3M), Spain, as a Principal Investigator of the CONnecting EXcellence (CONEX)- Plus Talent Training Program and Marie Skodowska-Curie Actions. During this Program he has spent two secondments at the: 1) Microwave Engineering Center for Space Applications (MECSA), Rome, Italy, from April to August 2024, and 2) SARAS Technology Ltd., Company, Leeds, U.K., from December 2022 to May 2023. In addition, during this program he had some short research visits at the: 1) University of Catania, Italy, in May 2024, along with an invited lecture entitled ‘‘Terahertz Antennas based on Metasurface and SIW’’ for the master’s and Ph.D. students, and postdoctoral researchers; 2) University of Messina, Italy, in May 2024; 3) University of Bradford, U.K., in May 2023; and 4) Edinburgh Napier University, U.K., in April 2023. For academic year 2021 and 2022, he received the ‘‘Teaching Excellent Acknowledgement’’ certificate for the course of ‘‘electromagnetic fields’’ from the Vice-Rector of studies of UC3M. In September 2024, he joined UNITOV, as a Senior Researcher. His research interests include electromagnetic systems, antennas and wave-propagations, metamaterials and metasurfaces, sensors, synthetic aperture radars (SAR), 5G and beyond wireless communications, multiple input multiple output (MIMO) systems, and RFID tag antennas, substrate integrated waveguides (SIWs),

Authorized licensed use limited to: London Metropolitan University. Downloaded on March 13,2025 at 11:16:28 UTC from IEEE Xplore. Restrictions apply.
© 2025 IEEE. All rights reserved, including rights for text and data mining and training of artificial intelligence and similar technologies. Personal use is permitted,
but republication/redistribution requires IEEE permission. See https://www.ieee.org/publications/rights/index.html for more information.

This article has been accepted for publication in IEEE Sensors Journal. This is the author's version which has not been fully edited and
content may change prior to final publication. Citation information: DOI 10.1109/JSEN.2025.3545789

impedance matching circuits, microwave components, millimeter-waves and terahertz integrated circuits, gap waveguide technology, beamforming networks, and reconfigurable intelligent surfaces (RIS),'' leading him to publish nine book chapters, more than 150 research articles in scientific journals, and more than 100 research papers in international conferences, including 47 in-person presentations in 29 conferences and 26 on-line presentations in 12 conferences. His research works received more than 7300 citations with H-index above 53 reported by Scopus, Google Scholar, and ResearchGate. According to Stanford University yearly analysis, he has been among the World's Top 2% Scientists of highly cited scientific authors, since 2020. He was listed in both Career Long and Single Year Impact in Stanford's list. He was a recipient of the two young engineer awards of the 47th and 48th European Microwave Conferences held in Nuremberg, Germany, in 2017, and in Madrid, Spain, in 2018, respectively. In April 2020, his research article entitled ''High-Gain Metasurface in Polyimide On-Chip Antenna Based on CRLH-TL for Sub Terahertz Integrated Circuits, Scientific Reports, volume 10, Article number 4298 (2020)'' was awarded as the Best Month Paper at the University of Bradford, U.K. He is an Editor of the book project entitled ''Wideband Wave-Propagating Components for Wireless RF Communications'' to be published by IntechOpen. In addition, he serves the role of an Associate Editor for two scientific journals of Radio Science and The Journal of Engineering (IET). He acts as a referee in several journals, and the technical program committee (TPC) and session chair of several international conferences. In addition, he is member of the reviewer panel of Dutch Research Council (NWO) and U.K. Research and Innovation (UKRI) Funding Service and the External Examiner of several Ph.D. dissertations from various worldwide universities.

Bal S. Virdee (SM'08) received the B.Sc. and MPhil degrees in Communications Engineering from the University of Leeds, UK, and his Ph.D. in Electronic Engineering from the University of London, UK. He has worked in industry for various companies including Philips (UK) as an R&D-engineer and Teledyne Defence and Space as a future products developer in RF/microwave communications. He has taught at several academic institutions before joining London Metropolitan University where he is a Senior Professor of Communications Technology in the School of Computing and Digital Media where he is Head the Communications Technology Research Center. His research, in collaboration with industry and academia, is in wireless communications encompassing mobile-phones to satellite-technology. Prof. Virdee has chaired technical sessions at IEEE international conferences and published numerous research papers. He is Executive Member of IET's Technical and Professional Network Committee on RF/Microwave-Technology. He is a Fellow of IET and a Senior-Member of IEEE.

Sunil Lavadiya working as Associate Professor in the Department of Information and Communication Technology at Marwadi University, Rajkot, Gujarat. He has completed his PhD on the topic of High Gain Frequency Reconfigurable Liquid Metamaterial Microstrip Patch Antenna. He has completed an M.Tech in communication engineering from Nirma University in 2010, and a B.Tech in Electronics and Communication from Saurashtra University in 2008. He has adapted to all aspects of Electronics and Communication Engineering, including training, education, and research. He works in the MIMO, Sensors, Reconfigurable, Superstrate, Solar absorber and liquid antennas. He is a member of professional bodies like IEEE and IETE. He has published 50 SCI research articles, 12 SCOPUS index articles, 8 book chapters, and 5 papers in an international conference and filed four design patents and one copyright.

Iftikhar ud din Received B.Sc. and M.Sc. Degree in Telecommunication Engineering from University of Engineering and Technology, Peshawar, Pakistan, in 2017 and 2021 respectively. He is the member of the Antennas & Microwave Engineering Research Group (AMERG) in UET Mardan. His current research interests include UWB antennas, FSS based UWB antennas and Sub-6 GHz 5G antennas, 5G millimeter wave antennas and MIMO antennas, frequency selective surfaces, EBGs and Metamaterial based antenna.

Bruno Cavalcante de Souza Sanches received the B.S. degree in information engineering and the M.Sc. degree in energy from the Federal University of ABC, Santo André, Brazil. He received the Ph.D. degree in microelectronics with the Integrated Systems Laboratory (LSI), University of São Paulo, São Paulo, Brazil, working in the design of a novel mixed signal integrated circuit used in the ALICE experiment in the CERN LHC. Bruno has more than fifteen years of experience in electronics and microelectronics design. He has been involved in hardware development, smart grids, algorithms, artificial intelligence, digital communication systems, EDA tools, electronics for high energy physics experiments and in several systems targeting early cancer detection including bioimpedance spectroscopy and microwave imaging.

SLAWOMIR KOZIEL received the M.Sc. and Ph.D. degrees in electronic engineering from Gdansk University of Technology, Poland, in 1995 and 2000, respectively. He also received the M.Sc. degrees in theoretical physics and in mathematics, in 2000 and 2002, respectively, as well as the PhD in mathematics in 2003, from the University of Gdansk, Poland. He is currently a Professor with the Department of Engineering, Reykjavik University, Iceland. His research interests include CAD and modeling of microwave and antenna structures, simulation-driven design, surrogate-based optimization, space mapping, circuit theory, analog signal processing, evolutionary computation and numerical analysis.

Syeda Iffat Naqvi (Senior Member, IEEE) received her PhD Telecommunication Engineering degrees from University of Engineering and Technology, Taxila, Pakistan, in 2021. She is currently serving as Assistant Professor at University of Engineering and Technology, Taxila. She is working towards the design and implementation of MIMO antennas systems for millimeter-wave 5G and beyond wireless communication applications, metamaterials, Terahertz and Sub-Terahertz antennas, Beamsteerable antenna arrays, and Ridge Gap Waveguide based antennas. She has authored and co-authored numerous technical articles in ISI-indexed journals, and deliver a number of conference talks. She is also a frequent reviewer of various prestigious journals. Furthermore, she has served as Technical Committee member for a number of international conferences and as Guest Editor for various Special Journal Issues.

Abinash Panda (Member, IEEE) received the B.Tech. and M.Tech. degrees in Electronics and Communication engineering from the Biju Patnaik University of Technology (BPUT), Odisha, India. Later, he pursued the Ph.D. degree from the National Institute of Technology, Silchar, Assam, India. He worked as a Postdoctoral researcher at Chulalongkorn University, Bangkok, Thailand. His research interests include photonic waveguides, photonic crystals, bio-photonic sensors, plasmonic sensors, optoelectronic devices, nanomaterial synthesis and characterization.

Ali Farmani (Member, IEEE) received the B.Sc. degree in electrical engineering from the Shiraz University of Technology in 2008, the M.Sc. degree in electrical engineering from the University of Tabriz in 2010, and the Ph.D. degree in electrical engineering from Shiraz University in 2017. During his stay at Lorestan University as an Assistant Professor (2018–2024), he has mentored several B.Sc., ten M.Sc. theses, and four Ph.D. dissertations. He is the author of more than 106 ISI papers and three book chapters. His research interests are VLSI, nanoelectronics, plasmonics, and investigation of new materials for integrated photonics. He was a recipient of the fellowship for Ph.D. study at Shiraz University as an Exceptional Talent. He received the Shiraz Distinguished Ph.D. Dissertation Award for his work on plasmonic nanostructures. He was also a recipient of the Excellent Reviewer Award from Elsevier and IEEE Journals (2017–2024).

Authorized licensed use limited to: London Metropolitan University. Downloaded on March 13,2025 at 11:16:28 UTC from IEEE Xplore. Restrictions apply.
© 2025 IEEE. All rights reserved, including rights for text and data mining and training of artificial intelligence and similar technologies. Personal use is permitted,
but republication/redistribution requires IEEE permission. See https://www.ieee.org/publications/rights/index.html for more information.

This article has been accepted for publication in IEEE Sensors Journal. This is the author's version which has not been fully edited and content may change prior to final publication. Citation information: DOI 10.1109/JSEN.2025.3545789

NASR RASHID was born in Egypt in 1973. He received the B.Sc. (with highest honors), M.Sc., and Ph.D. degrees in Electronics and Communication Engineering from Al-Azhar University, Cairo, Egypt, in 1996, 2004, and 2009, respectively. He is currently an Assistant Professor in the Department of Electrical Engineering at the College of Engineering, Jouf University, Sakaka, Saudi Arabia. His research interests include wireless communications, antennas and wave propagations, multiple-input multiple-output (MIMO) systems, impedance matching circuits, microwave components, and gap waveguide technology.

Lida Kouhalvandi, (M'17–SM'23), joined the Department of Electrical and Electronics Engineering at Dogus University as an Assistant Professor in October 2021 and she took possession of an Associate Professor degree in February 2023. She received her PhD in Electronics Engineering in 2021 from the Istanbul Technical University, Istanbul, Turkey. She received her MSc in Electronics Engineering in 2015 from the Istanbul Technical University, Istanbul, Turkey, and her BSc in Electronics Engineering in 2011 from the Azad University of Tabriz, Tabriz, Iran. In recognition of her research, she received a Doctoral Fellowship at the Department of Electronics and Telecommunications, Politecnico di Torino, Turin, Italy from 2019 to 2020, and she joined Politecnico di Torino, Turin, Italy as a Research Fellowship from February 2021 up to July 2021 and also from May 2022 up to May 2023. Her research interests as a radio frequency and analog engineer are power amplifiers, antenna, analog designs, and implantable medical devices. She also has experience in computer-aided designs and optimization algorithms through machine learning. Dr. Kouhalvandi has been a recipient of various awards. She received the 'Best Presentation Award' from the EExPolytech-2021: Electrical Engineering and Photonics conference in 2021. Additionally, her PhD thesis was accepted for presentation at the PhD Forum of the 2021 IEEE/ACM Design Automation Conference (DAC 2021) in San Francisco, USA. From the 30*th* IEEE conference on signal processing and communications applications, she received another 'Best Paper Award' in 2022. She received the 2022 Mojgan Daneshmand Grant from the IEEE Antennas and Propagation Society (AP-S), organized by the IEEE AP-S Young Professionals. Additionally, her PhD thesis was awarded by Istanbul Technical University as the 'Outstanding PhD Thesis' and also by the Turkish Electronics Industrialists Association (TESID) as the 'Best Innovation and Creativity PhD Thesis' in 2022. In 2022 and 2023, she was awarded the 'Outstanding Reviewer' by the Radio Science journal. She also serves as a reviewer at various journals indexed by IEEE. Moreover, her conference paper presented at 2024 11th International Conference on Electrical and Electronics Engineering (ICEEE 2024) was awarded as the best of session.

Milad Shariatifar is currently a researcher at University of Rome Tor Vergata, Italy. He was a postdoctoral researcher at instituto de telecommunications, Aveiro, Portugal and University of Amirkabir, Tehran, Iran. He received a Ph.D. degree in electronic and Communication engineering from Shahed University of Tehran, Iran. His main research interest is the design of microwave circuits, especially power amplifier theory, design, efficiency improvement and linearization techniques. He has been a reviewer of several IEEE transactions and other journal papers.

Authorized licensed use limited to: London Metropolitan University. Downloaded on March 13,2025 at 11:16:28 UTC from IEEE Xplore. Restrictions apply.
© 2025 IEEE. All rights reserved, including rights for text and data mining and training of artificial intelligence and similar technologies. Personal use is permitted, but republication/redistribution requires IEEE permission. See https://www.ieee.org/publications/rights/index.html for more information.